What lithic clasts and lithic-rich facies can tell us about diatreme processes: an example at Round Butte, Hopi Buttes volcanic field, Navajo Nation, Arizona

Benjamin Latutrie[*], Pierre-Simon Ross

Institut national de la recherche scientifique, Centre Eau Terre Environnement, 490 rue de la Couronne, Québec (QC), G1K 9A9, Canada

* Corresponding author
E-mail addresses: Benjamin.Latutrie@ete.inrs.ca (B. Latutrie), rossps@ete.inrs.ca (P-S. Ross)

Keywords:

Maar-diatreme, Lithic clasts, Debris jets, Debris avalanches, Megablocks

Abstract

Round Butte (Hopi Buttes volcanic field, Arizona) exposes a diatreme 170-190 m across, 190 m below the pre-eruptive surface. The central part of the massif is 130-150 m in diameter, displaying 20-30 m-high subvertical cliffs. The well-known layer-cake stratigraphy of the sedimentary rocks of the Colorado Plateau permits identification of the largest lithic fragments preserved in the Round Butte diatreme. We define three main groups of pyroclastic facies: undisturbed beds, disturbed beds and non-bedded rocks. Two other minor facies groups were mapped: megablocks (blocks over 2 m in long axis), and small-volume debris avalanche deposits. Pyroclastic megablocks are finer grained and richer in lithic clasts than most diatreme rocks surrounding them. These pyroclastic megablocks are interpreted as subsided portions of the maar ejecta ring. Sedimentary megablocks originate either from above, or from the same level, relative to their current location, i.e. no megablock has a net upward displacement. Small-volume debris avalanche deposits are poorly sorted deposits resulting from gravitational destabilization of the surrounding country rocks into the syn-eruptive crater. Small-volume debris avalanches and individual megablock collapse are the main ways in which the crater grew in size laterally during the eruption.

We combine the componentry of the disturbed bedded pyroclastic facies, the non-bedded pyroclastic facies and the pyroclastic megablocks with a series of conceptual models for country rock fragmentation. This exercise further allows us to estimate diatreme wall slopes of 70° below the Bidahochi Formation to approximately the depth of the root zone around 440 m below the pre-eruptive surface. Lithic fragments at the current level of exposure come from elevations up to 190 m above (i.e., up to the pre-eruptive surface) and up to 250 m below (i.e., down to the root zone) their current locations. Pyroclastic units displaying the richest content of lithic clasts with a deep origin are typically the non-bedded facies interpreted to have formed from debris jets during the eruption.

1 Introduction

Maar-diatremes are small, typically short-lived, mainly phreatomagmatic monogenetic volcanoes (Lorenz, 1986, 2007; White and Ross, 2011 Valentine and White, 2012; Ross et al., 2017; Németh and Kósik, 2020) that are most commonly found in monogenetic volcanic fields around the world (e.g., Németh et al., 2012; Brown and Valentine, 2013; Kereszturi et al., 2014; Poppe et al., 2016; Cas et al., 2017). They are, after scoria cones, the second most abundant type of volcanoes on continents (Vespermann and Schmincke, 2000). From bottom to top, maar-diatreme volcanoes are composed of a feeder intrusion (Re et al., 2015, 2016; Muirhead et al., 2016; Le Corvec et al., 2018), a root zone (Clement, 1982; Lorenz and Kurszlaukis, 2007; Haller et al., 2017), a lower non-bedded diatreme (White, 1991; Lefebvre et al., 2013, 2016), a transition zone (Bélanger and Ross, 2018; Latutrie and Ross, 2019), an upper typically bedded diatreme (White, 1991; Gernon et al., 2013; Delpit et al., 2014; Latutrie and Ross 2020), a maar crater (Lorenz, 1973; White, 1991; Graettinger, 2018) and an ejecta ring (Self et al., 1980; White, 1991; Vazquez and Ort, 2006; Valentine et al., 2015).

Pyroclastic rocks that compose the maar-diatreme typically contain a high proportion of lithic clasts derived from the surrounding country rocks, especially in the ejecta ring (e.g., Németh et al., 2000; Raue, 2004; Valentine, 2012; Ort et al., 2018). In the literature on non-kimberlitic maar-diatremes, lithic clasts found in the ejecta ring have received greater attention (Ollier, 1967; Lorenz, 1973, 1975; Ross et al., 2011; Graettinger and Valentine, 2017) than those found in the diatreme (Lefebvre et al., 2013), mainly because ejecta rings have a better worldwide availability. However, diatremes potentially preserve a more complete record of the eruption, since not all explosions expel material to the ejecta ring (Ross et al., 2008a, 2008b; Valentine et al., 2014, 2017).

In the area of the Hopi Buttes volcanic field (HBVF), Colorado Plateau sedimentary rocks are gently dipping to flat-lying and their stratigraphy is well known (Billingsley et al., 2013). Four main sedimentary formations crop out, namely from north to south and top to bottom: the Bidahochi Formation, the Moenave Formation, the Chinle Formation and the Moenkopi Formation (Figs. 1, 2; Billingsley et al., 2013). These are well described in the literature, display a relatively constant thickness, and can be examined in situ for reference. Thus, large lithic clasts in Hopi Buttes diatremes can often be assigned to a specific origin or source depth. This makes the HBVF an excellent location to study the origin of the lithic clasts within diatreme pyroclastic deposits (Lefebvre et al., 2013; Latutrie and Ross 2019). Round Butte is a well exposed HBVF diatreme and its overall volcanology was described by Latutrie and Ross (2019).

Here, we document in detail two facies groups of Round Butte diatreme, the megablocks and the small-volume debris avalanche deposits (DADs), that represent a volumetrically minor, but genetically important, part of the volcano's evolution. We provide a detailed study of lithic clasts and lithic-rich facies in the whole diatreme through a dataset of componentry measurements on pyroclastic facies, acquired through the line count and point count methods in the field and petrographic point counts on thin sections. The advantage of studying these lithic clasts in detail, along with lithic-rich facies such as DADs and megablocks, is that since the ultimate source depth range of the lithic material is known, the net upward or downward displacement of lithic clasts and megablocks can be reconstructed. We compare the measured lithic proportions with a series of conceptual country rock fragmentation models for the Round Butte diatreme. This exercise helps constrain the diatreme size and shape, and better elucidate eruptive processes within the maar crater and diatreme, including upward movements of fragments through debris jets related to subsurface explosions, and downward movements through crater wall collapse, mass wasting, or subsidence (McClintock and White, 2006; Ross et al., 2008a, 2008b; Lefebvre et al., 2013; Delpit et al., 2014; Sweeney and Valentine, 2015).

2 Methods

Several days were spent reconnoitering the regional sedimentary stratigraphy in the areas of White Cone, Bidahochi Butte, Twin Peaks, Five Buttes, Holbrook and Winslow (Fig. 1b) to get familiar with the typical structures and textures of each sedimentary formation and member. We spent most of the time in the field on Round Butte because we wanted to closely map the massif, characterize and sample pyroclastic facies

of the diatreme and identify lithic fragments found in the diatreme.

2.1 Mapping and facies groups at Round Butte

Field work at Round Butte is described by Latutrie and Ross (2019). A geological map of Round Butte (Fig. 1c) and nine detailed cliff maps of 20-30 m-high subvertical cliffs surrounding the massif were produced (Figs. 3, 4 and Figs. S1.1 to S1.7 in Online Resource 1). Five groups of facies were defined: the undisturbed bedded pyroclastic group, the disturbed bedded pyroclastic group, the non-bedded pyroclastic group, the megablocks group and the small-volume DADs group. The first three groups were described and interpreted by Latutrie and Ross (2019) whereas the last two are addressed here, along with the componentry for all facies groups.

2.2 Componentry measurements

Two main types of fragments dominate in pyroclastic rocks: juvenile and lithic (White and Houghton, 2006). Lithic fragments are clasts generated by the fragmentation of pre-existing rocks and deposits (White and Houghton, 2006). Typical lithic clasts in volcanic fields include sedimentary rocks, unconsolidated sediments, crystalline bedrocks and solidified lavas or pyroclastic rocks from older volcanoes. In a maar-diatreme volcano, existing pyroclastic rocks or deposits within the diatreme or ejecta ring can also be recycled as clasts during the eruption, and are considered lithic. However, individual juvenile fragments that are recycled during the eruption are still classified as juvenile because they are almost indistinguishable from first-cycle juvenile clasts (White and Houghton, 2006).

In the field, two componentry methods were used to quantify the relative proportions of various types of fragments 4 mm or larger (i.e., medium lapilli to blocks and bombs) found in pyroclastic facies: line counts (modified from Lefebvre, 2013) and point counts (modified from Ross and White, 2006). The reason for using these two methods is that line counts are easier on subvertical cliffs, but point counts (called clast counts in some previous papers) are more commonly used in geology. Field point counts were done on a subset of line count sites to enable a comparison between the methods (Online Resource 2). In addition, we used petrographic point counts on selected thin sections during lab work.

Field line counts were performed at 43 sites. At each site, we used three horizontal 1 m-long lines, spaced vertically by 50 cm, to cover an area of 1 m^2. The lines were manifested by a measuring tape, along which fragment intersection lengths were determined, for all particles (juvenile, country rock lithic and tuff) greater than or equal to 4 mm. The rest of the material was classified as undifferentiated matrix/cement. The proportion of a certain component was defined as the sum of the intersection lengths, divided by the total length measured along the tape.

Field point counts were obtained at 15 sites already covered by line counts in order to compare these two methods (Online Resource 2). We used a 1 m^2 square net with a 10 cm mesh, allowing us to quantify 100 points per site. During these measurements, fragments greater or equal to 4 mm were classified into different componentry bins (juvenile, country rock lithic and tuff), and we counted the rest as either matrix or cement.

Thirty-two thin sections of pyroclastic rocks were prepared from hand samples taken in the field to characterize the matrix (particles smaller than 4 mm in this paper). Eighteen of these thin sections were point counted for componentry using the "JmicroVision 1.2.7" software (Roduit, 2007; https://jmicrovision.github.io/). To obtain the necessary images, we used two different methods. Ten thin sections were initially imaged using a mosaic of plane-polarized light photomicrographs taken with a petrographic microscope at a magnification of 2.5x. The remaining eight thin sections were imaged with a "PowerSlide 5000" photographic slide scanner at an optical resolution of 5000 dpi. We counted 450 points on each thin section and used the recursive grid setting of JmicroVision.

3 Regional setting

3.1 Hopi Buttes volcanic field (HBVF)

The HBVF covers 2300 km^2 in the south-central part of the Colorado Plateau (Fig. 1a, Williams, 1936; White, 1991 Lefebvre et al., 2013; Latutrie and Ross, 2019). Miocene volcanic remnants, representing over 300 edifices, are mainly maar-diatremes (White, 1991; Lefebvre et al., 2013, 2016; Latutrie and Ross, 2019, 2020), lava flows (Williams, 1936), intrusions (Re et al., 2015, 2016; Muirhead et al., 2016) and rarely scoria cones (White, 1991; Vazquez, 1998). The abundant phreatomagmatic activity was related to

the water-rich Miocene playas and ponds (White, 1990; Dallegge et al., 2003) and underground subhorizontal aquifers (for recent aquifers, see Hart et al., 2002). The current arid setting and the variable erosion level in the HBVF provide excellent exposure of all parts (from the ejecta ring to feeder intrusions) of maar-diatremes. Round Butte, the topic of this study, is a diatreme located in the southeastern portion of the field (Figs. 1b, 1c).

3.2 Sedimentary formations of the HBVF area

This section introduces the four main sedimentary formations and associated members found in the Round Butte area (southeastern part of the HBVF). We unconventionally describe the four formations from top to bottom, taking the point of view that elevation "zero" is the pre-eruptive surface at the time of volcanism, and that relevant thicknesses are best expressed as depths below this surface (Fig. 1).

The _Bidahochi Formation_ (Pliocene and Miocene, Tbl) was named by Reagan (1924, 1932) and formerly described by Repenning and Irving (1954), Shoemaker et al. (1962) and Dallegge et al. (2003). Billingsley et al. (2013) mainly mapped the lower mudstone/argillaceous sandstone member (Miocene) in the Hopi Buttes area. Around Round Butte, the Bidahochi Formation is inferred to have had a thickness of about 50 m (see log in Fig. 1). The Bidahochi Formation sediments that are well exposed at Bidahochi Butte, White Cone or Crazy Waters (Figs. 1b, 2a) are lacustrine in origin, poorly consolidated to unconsolidated and composed of white to greenish/yellowish-grey claystone, light-red to brown-red mudstone/siltstone and whitish-grey sandstone (Fig. 2b) with locally mixed levels displaying an enrichment of juvenile fragments and free pyroxene crystals derived from the HBVF volcanism. The Bidahochi Formation rests unconformably on the Moenave Formation.

The _Moenave Formation_ (Lower Jurassic, Jm) is around 120 m-thick at Twin Peaks, near Round Butte (Fig. 1). Rocks are bedded, jointed/fractured, orange red to light red, fine to coarse grained, siltstone/sandstone, commonly displaying low-angle cross-beds, and forming weathered slopes (Fig. 2c; Billingsley et al., 2013). White to greenish-white horizons, spots or stripes are commonly observed within these rocks. Because of the joints and fractures, Moenave rocks probably stored water as an aquifer at the time of the eruptions (White, 1991; Lefebvre et al., 2012). The Moenave Formation rests unconformably on the Chinle Formation.

The _Chinle Formation_ (Upper Triassic, TRc) is composed of three members from top to bottom (Repenning et al., 1969; Billingsley et al., 2013): the Owl Rock Member (TRco, Figs. 1, 2d), the Petrified Forest Member (TRcp, Figs. 1, 2e) and the Shinarump Member (TRcs, Figs. 1, 2f). The Owl Rock Member is mainly purple/pink in color and is 80 m-thick in the Five Buttes to Round Butte area, where it crops out well (Figs. 1, 2d). It is composed of nodular limestone interbedded with slope-forming purple, light-blue/red calcareous claystone, siltstone and sandstone. The contact with the underlying Petrified Forest Member is marked by the lowermost limestone bed of the Owl Rock Member (Billingsley et al., 2013). The Petrified Forest Member is the thickest member of the Chinle Formation (140 m-thick). This member is composed by multicolor mudstone/siltstone intercalated with lenses of yellow/white coarse grained sandstone and fragments of logs of petrified wood. Petrified Forest rocks are variably consolidated. This member forms badlands-type terrain, such as the Painted Desert area north of Winslow (Figs. 1, 2e). At the bottom, the Shinarump Member is 20 m-thick, composed of channelized coarse grained sandstone to conglomerate rich in pebbles and intercalated with siltstone and mudstones (Fig. 2f). The Shinarump Member crops out along Interstate 40 and north of Winslow near N Park Dr road (Fig. 1b). The Chinle Formation rests unconformably on the Moenkopi Formation.

The _Moenkopi Formation_ (Middle? to Lower Triassic) is composed of two members in the HBVF area, with the Holbrook/Moqui Member at the top and the lower sandstone member at the bottom (McKee, 1954; Billingsley et al., 2013). Holbrook/Moqui Member rocks are micaceous (mainly white micas) reddish/brown and rarely greenish-grey claystone, siltstone and sandstone displaying cross-bedding and cusp-type ripple marks (TRm, Figs. 1, 2g). This member is 40 m-thick and crops out in Holbrook. The lower sandstone member (up to 25 m-thick) consists of light-red to light-brown, fine grained calcareous siltstone/sandstone with crossbedding (Figs. 1, 2h). This member crops out south of Winslow near state highway 99 (Fig. 1b).

4 Round Butte massif overview

4.1 Summary of the three main pyroclastic facies groups

Round Butte exposes the remnant of a small (170-190 m in diameter) but complex maar-diatreme volcano. The erosion level of the surrounding plain is about 190 m below the pre-eruptive surface and the central part of the massif is 130-150 m in diameter displaying 20-30 m-high cliffs. White (1991) described the massif as the contact between the upper and the lower diatreme but recently Latutrie and Ross (2019) highlighted that Round Butte consists of an upper diatreme and a thick transition zone. The massif displays three main pyroclastic groups of facies (Latutrie and Ross, 2019). The disturbed bedded and non-bedded pyroclastic groups have subvertical contacts with each other, forming an alternation of non-bedded "invasive" columns and disturbed bedded "residual" columns (Figs. 3, S1.4; the term "column" is defined in Latutrie and Ross, 2019) whereas the undisturbed bedded group mainly sits on the top of the other two pyroclastic groups, above an unconformity (Figs. 3, 4, S1.1 to S1.7).

4.2 Megablocks

Round Butte massif includes three types of megablocks (blocks over 2 m in long axis, Fig. 5), described in Table 1: (i) sedimentary (Bidahochi, Moenave and Chinle) megablocks, (ii) pyroclastic megablocks and (iii) juvenile megablocks. They are mainly present in the disturbed bedded pyroclastic group and in the non-bedded pyroclastic group (Figs. 3, S1.4, S1.6, S1.7). Rare Moenave Formation megablocks occur in the undisturbed bedded pyroclastic group (e.g., Fig. S1.7). The sedimentary megablocks that occur within the DADs group are treated as part of this group (Figs. 3, 4).

4.3 Small-volume debris avalanche deposits (DADs)

The five facies interpreted as formed by small-volume DADs are described in Table 1 and Fig. 6. Four of the five facies (aMBm, aMBp, aBB and aBBp) constitute the main DAD in the southwest side of the massif (Figs. 3, 4, S1.7) whereas the last facies (aTBh) forms multiple minor DADs on the west side (Fig. S1.6). DADs facies are named this way mainly because they are lithic-rich, poorly sorted (Figs. 3, 4), and interpreted as small debris avalanches within a volcanic crater, as discussed in detail below. The main DAD displays an inward dip of around 35° (towards the centre of the diatreme) and forms a 10 m-thick package of sedimentary-dominated DAD facies with intercalations of disturbed bedded pyroclastic rocks (Figs. 3, 4). The various sedimentary-dominated facies consist of lapilli- to megablock-sized Moenave or Bidahochi fragments, in a matrix of fragmented sedimentary or pyroclastic material (Figs. 4, 6). The main DAD has a concordant upper contact with the disturbed bedded pyroclastic group (Figs. 3, 4) and is crosscut by a unit of non-bedded pyroclastic rocks (Fig. 3). The multiple minor DADs (aTBh, Fig. S1.6) have a discordant lower contact with disturbed bedded pyroclastic rocks and the non-bedded pyroclastic rocks, and are conformably overlain by rocks of the undisturbed bedded pyroclastic group.

5 Componentry

5.1 Field line counts

Field line counts were carried out at 20 sites in disturbed bedded pyroclastic rocks, 17 sites in non-bedded pyroclastic rocks, and six sites in pyroclastic megablocks (Table 2). No line counts were done in the undisturbed bedded pyroclastic facies because this group is inaccessible, high in the cliffs. The mean proportion of undifferentiated matrix + cement is smallest (68%) in the non-bedded pyroclastic rocks, intermediate (74%) in the disturbed bedded rocks, and largest (83%) in the pyroclastic megablocks (Fig. 7). In other words, the non-bedded pyroclastic rocks are the coarsest grained, and the pyroclastic megablocks are the finest grained of the studied facies groups.

The Mann-Witney U test is a non-parametric statistical test, partly equivalent to a t-test comparing two sample means (Davis, 2002). Here the 'samples', in a statistical sense, are the groups of line counts from two facies. The Mann-Witney U test does not specifically test for a difference in means, but in general terms, answers the same geological question, i.e. are the facies really different? The null hypothesis, the alternative hypothesis, and the significance level are given in Table 3. The Mann-Witney U test confirms that the difference of the distribution of undifferentiated matrix + cement percentage between the pyroclastic megablocks and the other facies groups is statistically significant at the

95% level (Table 3, letter 'Y'). However, given the low number of measured sites, there is not enough information to confirm statistically that the non-bedded pyroclastic rocks are indeed coarser than the disturbed bedded rocks.

We also recalculated to 100% the proportions of juvenile (J) versus country rock lithic fragments (L) among clasts larger than or equal to 4 mm, to better compare the componentry of different groups of facies. This is expressed as the L/(L+J) ratio (Table 2, Fig. 7). No standard deviations are provided for this ratio here because we did not perform repeat analyses and no theoretical equation is available in the literature to estimate it, unlike for point counts. On average, in line counts, facies from the disturbed bedded pyroclastic group contain 75% juvenile clasts (25% country rock lithic clasts) whereas facies from the non-bedded pyroclastic group contain 84% juvenile clasts (16% country rock lithic clasts). Pyroclastic megablocks contain fewer juvenile clasts, 73% on average (27% country rock lithic clasts) within the counted fragments. Most of these differences are not statistically significant, except the lithic enrichment in the disturbed bedded group relative to the non-bedded group (Table 3, letter 'Y'). Country rock lithic clasts originate mainly from the Bidahochi and Moenave Formations, whereas Chinle and Moenkopi Formations clasts are found in trace proportions (Table 2); this is discussed in more detail below.

5.2 Field point counts

Field point counts were carried out at five sites in disturbed bedded pyroclastic rocks, seven sites in non-bedded pyroclastic rocks and three sites in pyroclastic megablocks (Table 4). No point counts were done in the undisturbed bedded pyroclastic facies because this group was unreachable. The mean matrix + cement proportion is the highest (80%) in the pyroclastic megablocks, intermediate (63%) in the disturbed bedded rocks and the lowest (60%) in the non-bedded pyroclastic rocks (Fig. 7). Again, the pyroclastic megablocks are the finest grained of the studied facies groups at Round Butte and the non-bedded pyroclastic rocks are the coarsest grained, on average.

The proportion of juvenile versus country rock lithic clasts among clasts larger than or equal to 4 mm was recalculated to 100% for the different groups of facies

(Table 4, Fig. 7). On average, the non-bedded pyroclastic rocks are the richest in juvenile clasts with 81% (19% country rock lithic clasts) whereas facies of the disturbed bedded group display an intermediate value of 71% (29% country rock lithic clasts) and the pyroclastic megablocks are the poorest in juvenile clasts with 67% (33% country rock lithic clasts). These averages are not directly comparable to those of the line count method because there are more line counts than field point counts, but we compare the data acquired by both methods at the same 15 sites in Online Resource 2.

The Mann-Witney U test does not confirm statistically significant differences in the distribution of matrix + cement or the proportion of country rock lithic versus juvenile clasts L/(L+J) between the disturbed bedded rocks, non-bedded rocks and pyroclastic megablocks (Table 3). This is probably due to low count numbers (100 points counted per site in total, including an effective number of points, n_{eff}, of 15 to 52 points actually falling in juvenile or country rock lithic clasts 4 mm or more); small numbers of sites studied; and internal variability within the facies groups. For the field point counts, theoretical estimates of the counting error are provided for the ratio L/(L+J) using the van der Plas and Tobi (1965) equation for standard deviation (Table 4). This highlights relatively high standard deviation values caused by the low n_{eff}.

5.3 Petrographic point counts

Whereas the field componentry methods focused on large clasts (≥4 mm), the petrographic point counts provide componentry information on the matrix (clasts <4 mm). We point-counted six thin sections (27x46 mm in size) of bedded pyroclastic rocks, nine of non-bedded pyroclastic rocks and three of pyroclastic megablocks (Table 5). No data are available for the undisturbed bedded pyroclastic group because we were unable to access and sample it. The "unresolved" column in Table 5, ranging from 6% to 50%, represents very fine grained material that could not be assigned to a specific category based on petrography; it probably consists of a mixture of altered juvenile ash and sedimentary mud. This abundance of very fine components in most samples confirms the poorly sorted nature of the rocks.

When only the known juvenile and country rock lithic clasts are considered and the total is recalculated to

100% (Table 5), juvenile fragments represent 87% of the counted clasts in the disturbed bedded group, on average (13% country rock lithic clasts), 90% of the non-bedded group (10% country rock lithic clasts), and 79% of pyroclastic megablocks (21% country rock lithic clasts). Table 3 highlights results of the Mann-Witney U test only on the proportion of country rock lithic clasts L/(L+J) because the category matrix + cement is not applicable to the petrographic point counts. The Mann-Witney U test did not confirm that these differences are statistically significant. Similarly to field point counts, we provide the same theoretical estimate of counting error on the L/(L+J) ratio (Table 5). Standard deviation values are lower than in field point counts because we acquired more points during the petrographic point counts, resulting in much higher n_{eff} values. A calcite-rich cement is present with the mean modal proportion at 8% and a range from near 0% to 23%.

6 Types of lithic clasts

6.1 Country rock lithic clasts

The most commonly identified country rock lithic clasts within the Round Butte massif are from the Bidahochi and Moenave Formations, i.e. from stratigraphic levels equal to, or higher than, the current elevation of the fragments in the diatreme. Chinle and Moenkopi clasts are much less common, and travelled mostly upward or stayed at the same level (e.g., Owl Rock Member of the Chinle Formation) relative to their original locations (Fig. 1). Some of the lithic clasts could not be assigned to a specific formation and some unassigned clasts may have a deeper origin (Billingsley et al., 2013).

Some juvenile-rich Bidahochi clasts consist of finely bedded sandstone composed of juvenile clasts in a fine muddy whitish matrix (Fig. 8a). However, most Bidahochi fragments are whitish to purplish fine sandstone as well as whitish, reddish or greenish mudstone (Figs. 5b, 5d, 6e, 6f, 8b), without obvious juvenile constituents. The size of Bidahochi fragments ranges from ash (disaggregated sedimentary particles within the matrix of pyroclastic rocks) to megablocks (Fig. 3). Sandstone fragments are angular in shape whereas the liquefied to brecciated mudstone clasts are sub-rounded to amoeboid (Figs. 3, 5d, 6e, 6f, 8a, 8b).

Moenave clasts are angular to sub-rounded with a size from coarse ash to megablocks. They are orange with occasional white spots or lines and are composed of competent fine sandstone to siltstone (Figs. 3, 5a, 6a, 8c).

Chinle clasts are present in the diatreme with sizes ranging from ash to megablocks. Owl Rock Member clasts are the most obvious in the massif and Owl Rock megablocks are observable in the diatreme margins (Fig. 1c). Identifiable Owl Rock clasts in the massif are mostly from competent interbeds of light-purple limestone with a sub-rounded to angular shape (Fig. 8d). Siltstone clasts within the massif originate from the Owl Rock or the Petrified Forest Members. Petrified Forest clasts are mostly multicolored siltstones (Fig. 8e). Shinarump Member fragments are white to yellowish, medium to coarse sandstone (Fig. 8f).

Angular clasts from the Holbrook Member of the Moenkopi Formation are present (Tables 2, 4). They are purplish-brown to greenish-grey fine sandstone to siltstone, mainly composed of quartz and micas (Fig. 8g). Clasts of the lower sandstone member of the Moenkopi Formation are not identifiable, either because they are absent or because they look like the Moenave Formation clasts.

6.2 Tuff clasts

Rare clasts of tuff have been found within coarser pyroclastic rocks in the diatreme. They are light brown to purplish-beige and are mainly sub-rounded to rarely angular in shape. These recycled tuff clasts are composed of juvenile and lithic fragments, often including Moenave clasts (Fig. 8h), and are classified as lithic clasts in the White and Houghton (2006) scheme. The distinction between these tuff clasts and the Bidahochi Formation clasts rich in juvenile fragments is based on the proportion of juvenile clasts (more abundant in the tuff fragments) versus pale sediment (more abundant in the Bidahochi Formation clasts). Also, Moenave clasts are only typically found within the tuff fragments and juvenile-rich Bidahochi fragments are commonly finely bedded (Fig. 8a).

7 Country rock fragmentation models of Round Butte

In this section we present conceptual models of country rock fragmentation during crater and diatreme formation at Round Butte. We calculate the 'theoretical' proportions of country rock lithic

fragments expected from different fragmentation and mixing models (Fig. 9) to compare them with our componentry measurements. This is a forward modeling approach in which we vary the diatreme wall angles and degrees of mixing, calculate the percentages of different sedimentary formations at the current depth of exposure (190 m below the pre-eruptive surface), and then compare these results with the componentry data obtained in the field. This exercise helps to constrain the approximate shape and volume of the diatreme, and its eruptive history, including for the unexposed and eroded portions.

7.1 Model parameters

Using modeling similar to that of Valentine (2012) for Dry Lake maar (San Francisco volcanic field, Arizona) or Lefebvre et al. (2013) for West Standing Rocks (HBVF), we calculated the 'theoretical' volumes and proportions of each sedimentary formation fragmented during the creation of the syn-eruptive crater and diatreme at Round Butte (Table 6 and Fig. 9). Thicknesses of the different sedimentary formations were derived from our observations around Round Butte and from regional observations of Billingsley et al. (2013), as compiled in the stratigraphic log (Fig. 1). The modeled fragmentation volume represents the crater and diatreme at the end of the eruption. Field observations show that the diatreme is 180 m in diameter at 190 m below the pre-eruptive surface and this is incorporated into the models (green dashed lines in Fig. 9).

We vary two parameters, the degree of mixing of the different sedimentary formations within the fragmentation volume, and the diatreme wall angles. For illustrative purposes, mixing ranges from nil (formations are brecciated but stay in place) to full (the diatreme is completely homogenized with respect to lithic proportions), representing extreme end-member cases. We explored a range of scenarios for diatreme wall slopes in the Bidahochi and underlying formations. Only the two most relevant scenarios, 1 and 2, are presented in Table 6 and Fig. 9. Wall slopes in the Bidahochi Formation are either 20° (observed at Twin Peaks) or 60° (used by Lefebvre et al., 2013) to cover a wide range of possibilities but still reflect the idea that the Bidahochi Formation was unconsolidated and easily excavated at the time of volcanism. Lefebvre et al. (2013) used 80° for wall slopes in the underlying formations at West Standing

Rocks, and wall slope observations at nearby Twin Peaks range from 70° to 88° (Latutrie and Ross, 2020). Wall slopes of 70° for Round Butte create cones that reach more plausible stratigraphic depths based on lithic componentry data, as discussed below. The Moenave and Moenkopi Formations were consolidated and competent at the time of volcanism, forming steep diatreme walls, whereas the Chinle Formation is variably consolidated, but for simplicity we assumed the same steep walls as in the Moenave and Moenkopi Formations, i.e. a perfect cone. This implies that the Chinle Formation did *not* liquefy during the eruption, which could have led to the collapse of a Moenave Formation overhang. There is no evidence of Chinle Formation liquefaction at Round Butte.

7.2 Origin and proportion of country rock lithic clasts

Scenarios 1 and 2 were chosen because they imply that the root zone of the diatreme reaches down into the Moenkopi Formation, which is the deepest identified source of lithic clasts at the current level of exposure. Even deeper sourced fragments may be present at diatreme levels lower than the current exposures, but there is no obvious way to verify this, so this possibility is not considered further. Table 6 compares scenarios 1 and 2 with the line and point count results, recalculated to 100% country rock lithic clasts, without considering the undifferentiated lithic clasts or juvenile fragments.

The models with no mixing of different sedimentary formations in the diatreme imply 100% Owl Rock Member at 190 m depth. This is obviously very different from what is actually observed at this depth, so this end-member is not considered further. Instead we focus on comparing the other end-member, complete mixing, with our componentry data. This shows that at 190 m depth, the diatreme is depleted in Bidahochi and Chinle clasts, but enriched in Moenave and Moenkopi clasts, relative to the models with complete mixing (Fig. 9). Specifically, the fully mixed scenarios predict that the Bidahochi Formation should account for 33-47% of lithic clasts, depending on wall slopes. Yet the main facies groups at the current level of exposure are poorer in Bidahochi clasts. This depletion is partly explained by excavation of the early crater within the Bidahochi Formation and expulsion of this material towards the

ejecta ring. At Round Butte, the ejecta ring has been eroded, but preserved ejecta rings in the HBVF are known to be especially rich in Bidahochi material (e.g. Teshim maar, White, 1991; Lefebvre et al., 2013; or Triplets, Graettinger and Valentine, 2017). At Round Butte specifically, evidence for a Bidahochi-rich ejecta ring comes from the pyroclastic megablocks, which we interpret as parts of the ejecta ring recycled into the diatreme; they contain an average of 51% Bidahochi fragments (on a 100% lithics basis) in line counts (Fig. 9). Another factor explaining the Bidahochi depletion of the diatreme is that the Bidahochi Formation was poorly consolidated and prone to disaggregation, meaning that some loose grains are hidden in the matrix of the pyroclastic rocks (Graettinger and Valentine, 2017). One last factor explaining the difference between actual componentry and our models is that the diatreme is not perfectly mixed.

For the Moenave Formation, the fully mixed model scenarios predict a 36-45% contribution to the country rock lithic assemblage. The line counts show much higher measured Moenave contents on a 100% country rock lithic clasts basis. The Moenave Formation is composed of competent sandstones to siltstones that are resistant to disaggregation after fragmentation, leading to the apparent enrichment in the diatreme (at the current exposure). Another possible factor to explain the abundance of Moenave clasts at 190 m depth is that mixing was incomplete, so that the upper part of stratigraphy is still comparatively enriched within the upper and middle part of the diatreme. A final possible explanation is that the volume of actually fragmented Moenave Formation is greater than in our perfect cone, i.e. the diatreme is wider within the Moenave Formation than shown on Fig. 9.

The model scenarios predict that the Chinle Formation should account for 17-22% of country rock lithic clasts in our completely mixed diatreme. Line and point counts show under 5% Chinle material among the identified country rock lithic clasts. Most of the Chinle Formation is composed of poorly indurated sandstone, siltstone and mudstone, prone to disaggregation. We think that most Chinle lithic fragments were completely disaggregated and are now hidden in the matrix as sand grains or mud. The line count proportion of ~3% and the point count proportion of ~2% are largely explained by clasts derived from the rare competent limestone interbeds of the Owl Rock Member. These clasts are easy to identify and extremely resistant to disaggregation. Another possible factor leading to scarcity of identifiable Chinle clasts at the current level of exposure could be that the Chinle Formation clasts have not moved up very much, i.e mixing was incomplete. This implies that at, deeper levels in the diatreme, the Chinle proportions within the lithic population, or at least within the matrix, would be higher.

Finally, the Moenkopi Formation is only fragmented in a very narrow cone in the scenarios, yielding well under 1% of the country rock lithic population. Yet, on average, line and point counts show a much higher percentage in the diatreme than in the completely mixed diatreme model, mainly because the root zone of the diatreme may not be as pointy as the cone shape illustrated in Fig. 9. The fact that the Moenkopi sandstones are well consolidated and resist disaggregation during transport is another factor explaining the discrepancy.

8 Interpretation and discussion

8.1 Summary of the origin of the three main groups of facies

The three main groups of facies that form the Round Butte diatreme are mainly phreatomagmatic in origin (Latutrie and Ross, 2019). The undisturbed bedded pyroclastic group, at the top of the massif above the unconformity, is composed of numerous subhorizontal beds, centimeters- to several meters-thick, of heterolithic to juvenile-rich coarse tuff to tuff breccia (Figs. 3, 4). Such bedded deposits were emplaced on the syn-eruptive crater floor by multiple explosions and are typical of the upper diatreme (White, 1991; White and Ross, 2011). Their characteristics suggest deposition from proximal fallout, pyroclastic density currents (PDCs) or fallback (Ross et al., 2013). The disturbed bedded pyroclastic group is variably deformed and disturbed but it displays similarities with the undisturbed bedded pyroclastic group in terms of componentry and grain size (coarse tuff to tuff breccia; Figs. 3, 4. S1.2, S1.3). Remnants of bedding are subhorizontal to swirly. Latutrie and Ross (2019) considered that the disturbed and the undisturbed bedded groups originally formed in the same way. The bedding

disturbance resulted from syn-eruptive subsidence, liquefaction processes or the injection of debris jets. The non-bedded group of pyroclastic facies is coarser and richer in juvenile clasts than the other two, and is formed by subvertical columns (Figs. 3, S1,4) invading facies of the disturbed bedded group, which therefore constitute residual columns (Figs. 3, S1.4). The non-bedded invasive columns were emplaced from debris jets (Latutrie and Ross, 2019).

8.2 Megablocks

At Round Butte, sedimentary and pyroclastic megablocks together represent 4% of exposed rocks (Figs. 3, 5, S1.4). Sedimentary megablocks are pieces of sediments and sedimentary rocks from the Moenave and Bidahochi Formations that fell down into the crater during the eruption (Figs. 5a, 5b). Crater enlargement would have been due to gravitational instability and perhaps some large explosions (White, 1991; White and Ross, 2011; Latutrie and Ross, 2019).

The composite megablock has a coherent lava part and a pyroclastic part (Figs. 3, 5c, 5d). The coherent part is inferred to represent a piece of a dike (or other sheet-like intrusion) that has a peperitic transition with the pyroclastic rock on its right side. This seems similar to peperitic transitions observed at the contact between dikes and pyroclastic rocks at East Standing Rocks, HBVF (Lefebvre et al., 2016), or at French Butte and Arch Rocks (Hooten and Ort, 2002). The country rock lithic clasts in the pyroclastic part come exclusively from the Bidahochi Formation and are mixed with juvenile fragments. It is likely that some phreatomagmatic explosions occurred at shallow depth to form an initial crater within Bidahochi sediments. This would have produced the non-bedded pyroclastic mixture of Bidahochi and juvenile clasts now found in the composite megablock (Table 1). Therefore, the pyroclastic rocks in this megablock are inferred to be a remnant of some of the first deposits that filled the crater at Round Butte, i.e. the proto-diatreme. This proto-diatreme was then invaded by a coherent dike and peperite formed at the transition with the wet pyroclastic deposits.

Other pyroclastic megablocks are bedded to non-bedded (Table 1; Figs, 3, S1.4). Where bedding is preserved, it consists of centimeters- to meters-thick beds composed of coarse tuff to fine lapilli tuff (Figs. 5e, 5f). Bedded units require space to form (i.e. they do not tend to form in subterranean settings), so were likely deposited from PDCs or fallout. We interpret these pyroclastic megablocks as parts of the ejecta ring that collapsed during stages of crater widening. Preservation of bedding planes was likely favoured by high cohesion due to a high water content in the ejecta ring deposits (Sohn, 1996; Vazquez and Ort, 2006).

8.3 Small-volume debris avalanche deposits (DADs)

The minor debris avalanches on the west side of the massif were emplaced at the level of the unconformity and fill at least three channels (Table 1; Fig. S1.6). We propose that small slumps in the crater wall sent mixtures of Bidahochi and Moenave material, and perhaps some pyroclastic material from the ejecta ring, down the crater sides. The minor debris avalanches partly eroded existing pyroclastic deposits, forming channels and mixing with them. The unconformity is interpreted as one of the crater floor positions during the volcano's evolution. The unconformity formed at the end of an eruptive phase during which excavation dominated over infilling (Latutrie and Ross, 2019). This would have destabilized the crater walls and caused the small debris avalanches.

The main DAD consists of Bidahochi-rich and Moenave-rich facies with no evidence of mixing between them. This main avalanche deposit likely resulted from several distinct slumps that affected different parts of the crater wall, with deposition of pyroclastic rocks in between the slumping events (Figs. 3, 4, 6). Facies forming the Moenave-rich part of the main DAD are closely associated and probably emplaced during one event (Table 1). Indeed, the Moenave breccia with a pyroclastic matrix (aMBp, Table 1) is found at the bottom and top of Moenave breccia with a Moenave matrix (Table 1), suggesting that this part of the DAD was emplaced with a pure Moenave core surrounded by mixed parts composed of Moenave and pyroclastic materials. During the flow, the interior of the moving Moenave mass was preserved from mixing, whereas the bottom part mixed with the pyroclastic deposits at the sides and bottom of the crater. It is less clear how the aMBp found at the top formed. During the DAD emplacement, the front of the Moenave flow may have mixed with pyroclastic deposits in the diatreme

and a small part of this mixture was able to overbank on the top. The Bidahochi-rich part of the main DAD is composed of a main facies of Bidahochi breccia at the top, and a minor facies of Bidahochi breccia with a pyroclastic matrix at the bottom (Table 1). The main facies is bedded and is formed by many small Bidahochi mudflows that piled up. Locally, mudflows mixed with the fine to medium lapilli tuff to form the minor facies (Figs. 3, 4).

8.4 Implications for lithic transport within the diatreme

Country rock lithic clasts at Round Butte range from single mineral grains within the matrix of pyroclastic rocks to megablocks. The country rock lithic clasts found at the current level of exposure (190 m depth) originate from the Bidahochi, Moenave, Chinle (Owl Rock, Petrified Forest and Shinarump Members) and Moenkopi Formations. Fragments from the Bidahochi and Moenave Formations, and from the Owl Rock Member – including all sedimentary megablocks – have moved down by 0-190 m from their sources, into an occasionally deep crater. Fragments from the Petrified Forest Member, the Shinarump Member and the Moenkopi Formation are up to 20-30 cm across (no megablocks) and have a net upwards displacement of up to 250 m relative to their sources. The upward movement of these fragments is explained by debris jets resulting from phreatomagmatic explosions at various levels in the diatreme. One of the clearest manifestations of deeply sourced debris jets at Round Butte is the lithic-rich tuff breccia domain in Fig. 3. No point or line count was obtained for this location, but the rocks are extremely rich in clasts from the Chinle and Moenkopi Formations.

Since we explain the net upward movement of fragments from deeper formations with debris jets, and since no megablock has a net upward movement (at the current level of exposure), we conclude that debris jets could not permanently move megablocks upward. This could be related to the large mass of individual megablocks and the low density of debris jets but also to the large cross-sectional area of megablocks, implying the need to lift a significant amount of overlying pyroclastic material upward. Megablocks of deep sedimentary formations may be preserved at deeper levels at Round Butte.

Lefebvre et al. (2013) built a conceptual country rock fragmentation model for West Standing Rocks (WSR), another diatreme in the HBVF (Fig. 1). Their model is generally similar to ours and can be compared with what we obtained for Round Butte. They considered diatreme wall slopes of 60° in the Bidahochi Formation and 80° for the sedimentary rocks below. The WSR model suggests a diatreme around 700 m deep, 260 m deeper than for the Round Butte model. Within the WSR diatreme, at the current level of exposure, country rock lithic clasts are mainly derived from the Moenave Formation and the Owl Rock Member. Only traces of the other sedimentary formations and members are represented. For the depletion in Bidahochi Formation material, Lefebvre et al. (2013) also proposed that most of the Bidahochi Formation was expelled toward the ejecta ring and/or that Bidahochi material is hidden within the matrix of WSR pyroclastic units. The main difference between the WSR and the Round Butte models is the proportion of deep lithic clasts, derived from the Chinle Formation (Petrified Forest and Shinarump Members) and from the Moenkopi Formation. At WSR, despite the idea of a deeper diatreme, and despite the fact that the massif there crops out in the Petrified Forest Member (~110 m below the base of the Round Butte massif), deep lithic clasts are even less represented than at Round Butte. Lefebvre et al. (2013) proposed that those deep lithic clasts at WSR are likely preserved at a lower level within the country rock breccia. If the very steep wall slopes assumed by Lefebvre et al. (2013) for WSR are correct, the difference in deep lithic clast abundance relative to Round Butte could be the result of the variability of the intensity and number of the phreatomagmatic explosions, the location of the explosion sites, the size of the diatreme or the ability of deep rooted debris jets to move material up as discussed by Sweeney and Valentine (2015). Billingsley et al. (2013) highlighted that the Holbrook/Moqui Member of the Moenkopi Formation is formed by channels implying that this member is not uniformly present in the HBVF. This could be another explanation for the very low concentration of Moenkopi clasts because this formation was missing below WSR.

8.5 Country rock lithic clasts in the ejecta ring versus the diatreme

In the context of non-kimberlitic maar-diatremes, more studies have focused on country rock lithic clasts preserved in the maar ejecta ring (Ollier, 1967; Lorenz, 1973, 1975; White, 1991; Ross et al., 2011; Valentine, 2012; Graettinger and Valentine, 2017) than in the diatreme (Lefebvre et al., 2013; Latutrie and Ross, 2019). This is mainly due to the better worldwide availability and accessibility of maar ejecta rings, and the focus of many researchers on Quaternary, as opposed to older, volcanoes.

HBVF ejecta rings are rich in lithic clasts derived from the Bidahochi and Moenave Formations (White, 1991; Lefebvre et al., 2013; Graettinger and Valentine, 2017) but show little evidence of fragments derived from deep formations such as the Chinle or the Moenkopi. Studying maar ejecta rings rich in country rock lithic clasts with a shallow origin might lead to the idea of a shallow diatreme, perhaps with gentle wall slopes (Jordan et al., 2013). However, actual diatremes exposed in the HBVF tell a different story. For example, at Round Butte, clasts from four formations are contained within the exposed part of the diatreme, from the Bidahochi (at the pre-eruptive surface) to the Moenkopi (around 440 m below the pre-eruptive surface). Some fragments from even deeper formations may be present at diatreme levels lower than the current exposures. This study of the Round Butte diatreme shows that some country rock lithic fragments have moved up while others have moved down, relative to their sources.

Deep phreatomagmatic explosions, i.e. ~250 m deep or more, are typically not powerful enough to eject material to the atmosphere (Valentine et al., 2014; Sweeney and Valentine, 2015). Some debris jets remain constrained within the diatreme (when explosion sites are deeper than ~120 m, Valentine et al., 2014), forming subterranean "invasive columns" (Latutrie and Ross, 2019 and references therein). Lithic clasts with a deep origin will rarely reach the upper parts of the volcano (ejecta ring or upper diatreme), unless moved successively upwards by multiple debris jets (Valentine et al., 2014). In contrast, shallowly-sourced lithic clasts will probably be found only in low concentrations in the lower diatreme and root zone because they are preferentially expelled toward the ejecta ring, because of incomplete mixing, and because friable formations are sometimes disaggregated in small particles hiding in the matrix. Studying country rock lithic clasts in the diatreme shows that eruptive processes in the diatreme are more complex (Ross et al., 2008a, 2008b; Valentine et al., 2014, 2017) than expected when only looking at the ejecta ring.

9 Conclusions

We carried out a detailed study of lithic clasts and lithic-rich facies (small-volume DADs, sedimentary megablocks) in the Round Butte diatreme to better constrain its overall evolution and eruptive processes. The layer cake stratigraphy of the country rocks in the HBVF area allowed us to build country rock fragmentation models for Round Butte and to quantify 'theoretical' proportions of sedimentary formation fragmented, assuming either complete mixing of different formations in the diatreme or no mixing at all. Those proportions were then compared to field componentry measurements (line and point counts) in the pyroclastic rocks. We suggest that the root zone is located around 440 m below the pre-eruptive surface because no Paleozoic sedimentary rocks were found at the current level of exposure of Round Butte diatreme (although deeper sourced country rocks lithic clasts may be present at lower levels in the diatreme). This supports diatreme walls sloping around 70°, except in the Bidahochi Formation where they were gentler. Competent sedimentary rocks (Moenave Formation, Owl Rock Member and Moenkopi Formation) are better preserved as recognizable lithic clasts in the diatreme than the less competent stratigraphic units (Bidahochi Formation, Petrified Forest Member and Shinarump Member), which are largely disaggregated and contribute to the matrix of the pyroclastic rocks. Additionally, the Bidahochi Formation was preferentially excavated during crater development and expelled toward the ejecta ring. The Moenave Formation is abundant in the lithic population partly due to incomplete mixing of the lithic clasts within the diatreme, and perhaps because the diatreme may have been wider in the Moenave Formation than implied by our simple conical model. Fragments of deep formations travelled upwards within debris jets to the current exposure level inside the diatreme.

The main debris avalanche in the SW corner of Round Butte is the result of two crater wall slumps, one in the Moenave Formation and a second in the Bidahochi Formation. The smaller DADs on the west

side of the massif were formed slightly later, at the time the unconformity was generated. Beyond these mass movements of material from the crater walls, individual megablocks from the country rocks and ejecta ring fell regularly into the crater during the eruption, due to gravitational instability. Slumps and individual megablock collapse are the main mechanisms that enlarged the syn-eruptive crater laterally. We also highlight that no megablocks show a net upward movement, suggesting that debris jets are not able to move them upwards permanently.

Acknowledgements

References

Bélanger, C., Ross, P.-S., 2018. Origin of nonbedded pyroclastic rocks in the Cathedral Cliff diatreme, Navajo volcanic field, New Mexico. Bull Volcanol, 80: article 61.

Billingsley, G.H., Block, D., Hiza-Redsteer, M., 2013. Geologic map of the Winslow 30′× 60′ quadrangle, Coconino and Navajo Counties, northern Arizona, US Geol Surv Scientific Investigations, Map 3247, scale 1:50 000.

Brown, R.J., Valentine, G.A., 2013. Physical characteristics of kimberlite and basaltic intraplate volcanism and implications of a biased kimberlite record. Geol Soc Am Bull, 125: 1224-1238.

Cas, R.A.F., Van Otterloo, J., Blaikie, T.N., Van Den Hove, J., 2017. The dynamics of a very large intra-plate continental basaltic volcanic province, the Newer Volcanics Province, SE Australia, and implications for other provinces. Geol Soc, London, Special Publication, 446: 123-172.

Clement, C.R., 1982. A comparative geological study of some major kimberlite pipes in the Northern Cape and Orange Free State. PhD thesis: University of Cape Town, South Africa. 451p

Dallegge, T.A., Ort, M.H., Mcintosh, W.C., 2003. Mio-Pliocene chronostratigraphy, basin morphology and paleodrainage relations derived from the Bidahochi Formation, Hopi and Navajo Nations, northeastern Arizona. The Mountain Geologist, 40: 55-82.

Davis, J.C., 2002. Statistics and Data Analysis in Geology - Third Edition. John Wiley & Sons, New York. 638p

Delpit, S., Ross, P.-S., Hearn, B.C., 2014. Deep-bedded ultramafic diatremes in the Missouri River Breaks volcanic field, Montana, USA: 1 km of syn-eruptive subsidence. Bull Volcanol, 76: article 832.

Gernon, T.M., Upton, B.G.J., Hincks, T.K., 2013. Eruptive history of an alkali basaltic diatreme from Elie Ness, Fife, Scotland. Bull Volcanol, 75: article 704.

Graettinger, A.H., 2018. Trends in maar crater size and shape using the global Maar Volcano Location and Shape (MaarVLS) database. J Volcanol Geotherm Res, 357: 1-13.

Graettinger, A.H., Valentine, G.A., 2017. Evidence for the relative depths and energies of phreatomagmatic explosions recorded in tephra rings. Bull Volcanol, 79: article 88.

Haller, M.J., Ross, P.-S., White, J.D.L., Lefebvre, N.S., 2017. Overview of the Cerro Chivo volcanic field (CCVF), Chubut province, Argentina: Basalt sheets, root zones, diatremes and 'plugs'. In: XX Congreso

Geologico Argentino, San Miguel de Tucumàn, Argentina. 8p.

Hart, R.J., Ward, J.J., Bills, D.J., Flynn, M.E., 2002. Generalized hydrogeology and ground-water budget for the C aquifer, Little Colorado River Basin and parts of the Verde and Salt River Basins, Arizona and New Mexico. US Geol Surv Water-Resources Investigations Report: 02-4026.

Hooten, J.A., and Ort, M.H., 2002. Peperite as a record of early-stage phreatomagmatic fragmentation processes: an example from the Hopi Buttes volcanic field, Navajo Nation, Arizona, USA. J Volcanol Geotherm Res, 114: 95-106.

Jordan, S.C., Cas, R.A.F. and Hayman, P.C., 2013. The origin of a large (> 3 km) maar volcano by coalescence of multiple shallow craters: Lake Purrumbete maar, southeastern Australia. J Volcanol Geotherm Res, 254: 5-22.

Kereszturi, G., Németh, K., Cronin, S.J., Procter, J., Agustín-Flores, J., 2014. Influences on the variability of eruption sequences and style transitions in the Auckland Volcanic Field, New Zealand. J Volcanol Geotherm Res, 286: 101-115.

Latutrie, B., Ross, P.-S., 2019. Transition zone between the upper diatreme and lower diatreme: origin and significance at Round Butte, Hopi Buttes volcanic field, Navajo Nation, Arizona. Bull Volcanol, 81: article 26.

Latutrie, B., Ross, P.-S., 2020. Phreatomagmatic vs magmatic eruptive styles in maar-diatremes: a case study at Twin Peaks, Hopi Buttes volcanic field, Navajo Nation, Arizona. Bull Volcanol, 82: article 28.

Le Corvec, N., Muirhead, J.D., White, J.D.L., 2018. Shallow magma diversions during explosive diatreme-forming eruptions. Nat Commun, 9: 1459.

Lefebvre, N.S., 2013. Volcanology of maar-diatreme volcanic vent complexes, Hopi Buttes Volcanic Field, Navajo Nation, Arizona, USA. PhD thesis: University of Otago, New Zealand. 269p

Lefebvre, N.S., White, J.D.L., Kjarsgaard, B.A., 2012. Spatter-dike reveals subterranean magma diversions: Consequences for small multivent basaltic eruptions. Geology, 40: 423-426.

Lefebvre, N.S., White, J.D.L., Kjarsgaard, B.A., 2013. Unbedded diatreme deposits reveal maar-diatreme-forming eruptive processes: Standing Rocks West, Hopi Buttes, Navajo Nation, USA. Bull Volcanol, 75: 1-17.

Lefebvre, N.S., White, J.D.L., Kjarsgaard, B.A., 2016. Arrested diatreme development: Standing Rocks East, Hopi Buttes, Navajo Nation, USA. J Volcanol Geotherm Res, 310: 186-208.

Lorenz, V., 1973. On the formation of maars. Bull Volcanol, 37: 183-204.

Lorenz, V., 1975. Formation of phreatomagmatic maar-diatreme volcanoes and its relevance to kimberlite diatremes. Physics and Chemistry of the Earth, 9: 17-27.

Lorenz, V., 1986. On the growth of maars and diatremes and its relevance to the formation of tuff rings. Bull Volcanol, 48: 265-274.

Lorenz, V., 2007. Syn-and posteruptive hazards of maar–diatreme volcanoes. J Volcanol Geotherm Res, 159: 285-312.

Lorenz, V., Kurszlaukis, S., 2007. Root zone processes in the phreatomagmatic pipe emplacement model and consequences for the evolution of maar–diatreme volcanoes. J Volcanol Geotherm Res, 159: 4-32.

McClintock, M,. White, J.D.L., 2006. Large phreatomagmatic vent complex at Coombs Hills, Antarctica: wet, explosive initiation of flood basalt volcanism in the Ferrar-Karoo LIP. Bull Volcanol, 68: 215-239.

McKee, E.D., 1954. Stratigraphy and history of the Moenkopi Formation of Triassic age. Geol Soc Am Memoir 61.

Muirhead, J.D., Van Eaton, A.R., Re, G., White, J.D.L., Ort, M.H., 2016. Monogenetic volcanoes fed by interconnected dikes and sills in the Hopi Buttes volcanic field, Navajo Nation, USA. Bull Volcanol, 78: 1-16.

Németh, K., Kósik, S., 2020. Review of explosive hydrovolcanism. Geosciences, 10: 44.

Németh, K., Cronin, S.J., Smith, I.E.M., Augustin Flores, J., 2012. Amplified hazard of small-volume monogenetic eruptions due to environmental controls, Orakei Basin, Auckland Volcanic Field, New Zealand. Bull Volcanol, 74: 2121-2137.

Nemeth, K., Martin, U., Harangi, S., 2000. On the calculation of the geometry of the diatreme pipe from a deposits of an" accidental lithic clast rich" maar, Tihany East Maar (Hungary). Terra Nostra: 383-390.

Ollier, C.D., 1967. Maars their characteristics, varieties and definition. Bull Volcanol, 31: 45-73.

Ort, M.H., Lefebvre, N.S., Neal, C.A., McConnell, V.S., Wohletz, K.H., 2018. Linking the Ukinrek 1977 maar-eruption observations to the tephra deposits: New insights into maar depositional processes. J Volcanol Geotherm Res, 360: 36-60.

Poppe, S., Smets, B., Fontijn, K., Rukeza, M.B., Migabo, A.D.M.F., Milungu, A.K., Namogo, D.B., Kervyn, F., Kervyn, M., 2016. Holocene phreatomagmatic eruptions alongside the densely populated northern shoreline of Lake Kivu, East African Rift: timing and hazard implications. Bull Volcanol, 78: article 82.

Raue, H., 2004. A new model for the fracture energy budget of phreatomagmatic explosions. J Volcanol Geotherm Res, 129: 99-108.

Re, G., White, J.D.L., Muirhead, J.D., Ort, M.H., 2016. Subterranean fragmentation of magma during conduit initiation and evolution in the shallow plumbing system of the small-volume Jagged Rocks volcanoes (Hopi Buttes Volcanic Field, Arizona, USA). Bull Volcanol, 78: article 55.

Re, G., White, J.D.L., Ort, M.H., 2015. Dikes, sills, and stress-regime evolution during emplacement of the Jagged Rocks complex, Hopi Buttes Volcanic field, Navajo Nation, USA. J Volcanol Geotherm Res, 295: 65-79.

Reagan, A.B., 1924. Stratigraphy of the Hopi Buttes volcanic field, Arizona. Pan-American Geologist, v. 41, p. 355-366.

Reagan, A.B., 1932. The Tertiary-Pleistocene of the Navajo Country in Arizona, with a description of some of its included fossils. Transact Kansas Acad Sci, 35: 253-259.

Repenning, C.A., Irwin, J.H., 1954. Bidahochi Formation of Arizona and New Mexico. AAPG Bull, 38: 1821-1826.

Repenning, C.A., Cooley, M.E., Akers, J.P., 1969. Stratigraphy of the Chinle and Moenkopi formations, Navajo and Hopi Indian reservations; Arizona, New Mexico, and Utah. 2330-7102, US Geol Profess Pap 521–B.

Roduit, N., 2007. JMicroVision: un logiciel d'analyse d'images pétrographiques polyvalent, PhD thesis: University of Geneva, Switzerland, 129 p

Ross, P.-S., White, J.D.L., 2006. Debris jets in continental phreatomagmatic volcanoes: a field study of their subterranean deposits in the Coombs Hills vent complex, Antarctica. J Volcanol Geotherm Res, 149: 62-84.

Ross, P.-S., White, J.D.L., Zimanowski, B., Büttner, R., 2008a. Multiphase flow above explosion sites in debris-filled volcanic vents: Insights from analogue experiments. J Volcanol Geotherm Res, 178: 104-112.

Ross, P.-S., White, J.D.L., Zimanowski, B., Büttner, R., 2008b. Rapid injection of particles and gas into non-fluidized granular material, and some volcanological implications. Bull Volcanol, 70: 1151-1168.

Ross, P.-S., Delpit, S., Haller, M.J., Németh, K., Corbella, H., 2011. Influence of the substrate on maar–diatreme volcanoes—an example of a mixed setting from the Pali Aike volcanic field, Argentina. J Volcanol Geotherm Res, 201: 253-271.

Ross, P.-S., White, J.D.L., Valentine, G.A., Taddeucci, J., Sonder, I., Andrews, R.G., 2013. Experimental birth of a maar–diatreme volcano. J Volcanol Geotherm Res, 260: 1-12.

Ross, P.-S., Carrasco-Núñez, G., Hayman, P., 2017. Felsic maar-diatreme volcanoes: a review. Bull Volcanol, 79: article 20.

Self, S., Kienle, J., Huot, J.-P., 1980. Ukinrek Maars, Alaska, II. Deposits and formation of the 1977 craters. J Volcanol Geotherm Res, 7: 39-65.

Shoemaker, E.M., Roach, C.H., Byers, F.M.J., 1962. Diatremes and uranium deposits in the Hopi Buttes, Arizona. Petrologic Studies—A Volume in Honor of AF Buddington: Boulder, Colorado, Geol Soc Am: 327-355.

Sohn, Y.K., 1996. Hydrovolcanic processes forming basaltic tuff rings and cones on Cheju Island, Korea. Geol Soc Am Bull, 108: 1199-1211.

Sweeney, M.R., Valentine, G.A., 2015. Transport and mixing dynamics from explosions in debris-filled volcanic conduits: numerical results and implications for maar-diatreme volcanoes. Earth Planet Sci Lett, 425: 64-76.

Valentine, G.A., 2012. Shallow plumbing systems for small-volume basaltic volcanoes, 2: Evidence from crustal xenoliths at scoria cones and maars. J Volcanol Geotherm Res, 223: 47-63.

Valentine, G.A., White, J.D.L., 2012. Revised conceptual model for maar-diatremes: Subsurface processes, energetics, and eruptive products. Geology, 40: 1111-1114.

Valentine, G.A., Graettinger, A.H., Sonder, I., 2014. Explosion depths for phreatomagmatic eruptions. Geophys Res Lett, 41: 3045-3051.

Valentine, G.A., Sottili, G., Palladino, D.M., Taddeucci, J., 2015. Tephra ring interpretation in light of evolving maar–diatreme concepts: Stracciacappa maar (central Italy). J Volcanol Geotherm Res, 308: 19-29.

Valentine, G.A., White, J.D.L., Ross, P.-S., Graettinger, A.H., Sonder, I., 2017. Updates to concepts on phreatomagmatic maar-diatremes and their pyroclastic deposits. Frontiers Earth Sci, 5: 68.

Van der Plas, L., Tobi, A.C., 1965. A chart for judging the reliability of point counting results. Am J Sci, 263: 87-90.

Vazquez, J.A., 1998. Maar volcanism in the Wood Chop Mesa area, Hopi Buttes volcanic field, Navajo Nation, Arizona. MSc thesis: University of Northern Arizona, USA. 221p

Vazquez, J.A., Ort, M.H., 2006. Facies variation of eruption units produced by the passage of single pyroclastic surge currents, Hopi Buttes volcanic field, USA. J Volcanol Geotherm Res, 154: 222-236.

Vespermann, D., Schmincke, H.-U., 2000. Scoria cones and tuff rings, Encyclopedia of volcanoes. Elsevier first edition. Academic Press, pp. 683-694.

White, J.D.L., 1990. Depositional architecture of a maar-pitted playa: sedimentation in the Hopi Buttes volcanic field, northeastern Arizona, USA. Sediment Geol, 67: 55-84.

White, J.D.L., 1991. Maar-diatreme phreatomagmatism at Hopi Buttes, Navajo Nation (Arizona), USA. Bull Volcanol, 53: 239-258.

White, J.D.L., Houghton, B.F., 2006. Primary volcaniclastic rocks. Geology, 34: 677-680.

White, J.D.L., Ross, P.-S., 2011. Maar-diatreme volcanoes: a review. J Volcanol Geotherm Res, 201: 1-29.

Williams, H., 1936. Pliocene volcanoes of the Navajo-Hopi country. Geol Soc Am Bull, 47: 111-172.
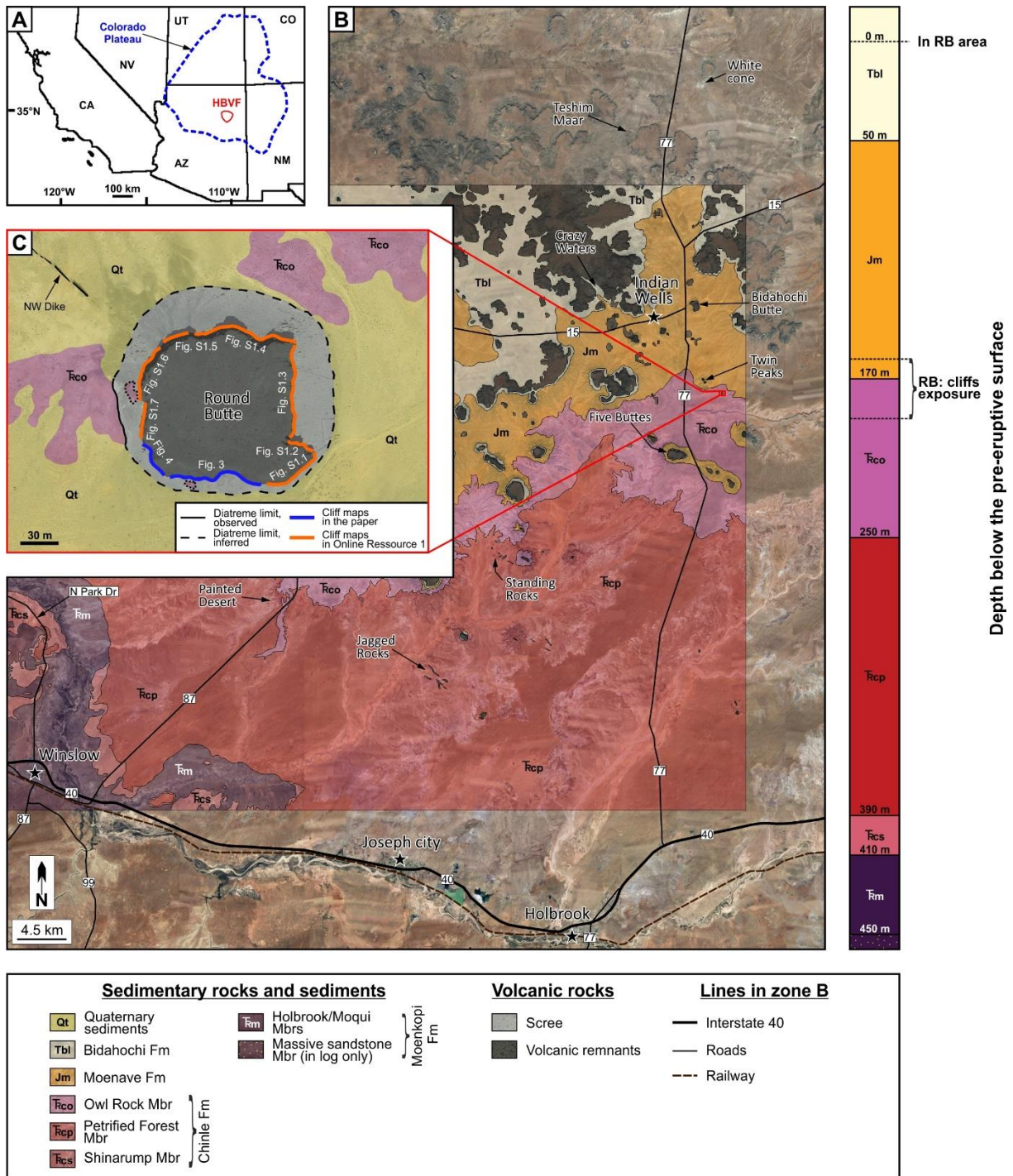
Figure 1 Maps displaying A) the location of the Colorado Plateau and the HBVF, B) geology of a portion of the HBVF (map centre at UTM zone 12S, 572 410 m E, 3 916 058 m N), simplified from Billingsley et al. (2013) and C) a close-up of the Round Butte diatreme (map centre at 588 158 m E, 3 910 326 m N). The sedimentary log displays the inferred thickness of the sedimentary formations in the Round Butte (RB) area.

Figure 2 Photo plate of the main sedimentary formations in the HBVF area. A) General view of the Bidahochi Formation at White cone, B) Bidahochi Formation at Crazy Waters (photo by J.D.L. White, 2012) displaying the bedding formed by mudstone/siltstone and argillaceous sandstone, C) Moenave Formation at Twin Peaks, D) Owl Rock Member of the Chinle Formation south of Five Buttes, E) Petrified Forest Member of the Chinle Formation in the Painted Desert area north of Winslow, F) Shinarump Member of the Chinle Formation close to the N Park Dr road, north of Winslow, G) Holbrook/Moqui Member of the Moenkopi Formation in Holbrook city and H) lower sandstone member of the Moenkopi Formation close to state highway 99, south of Winslow.
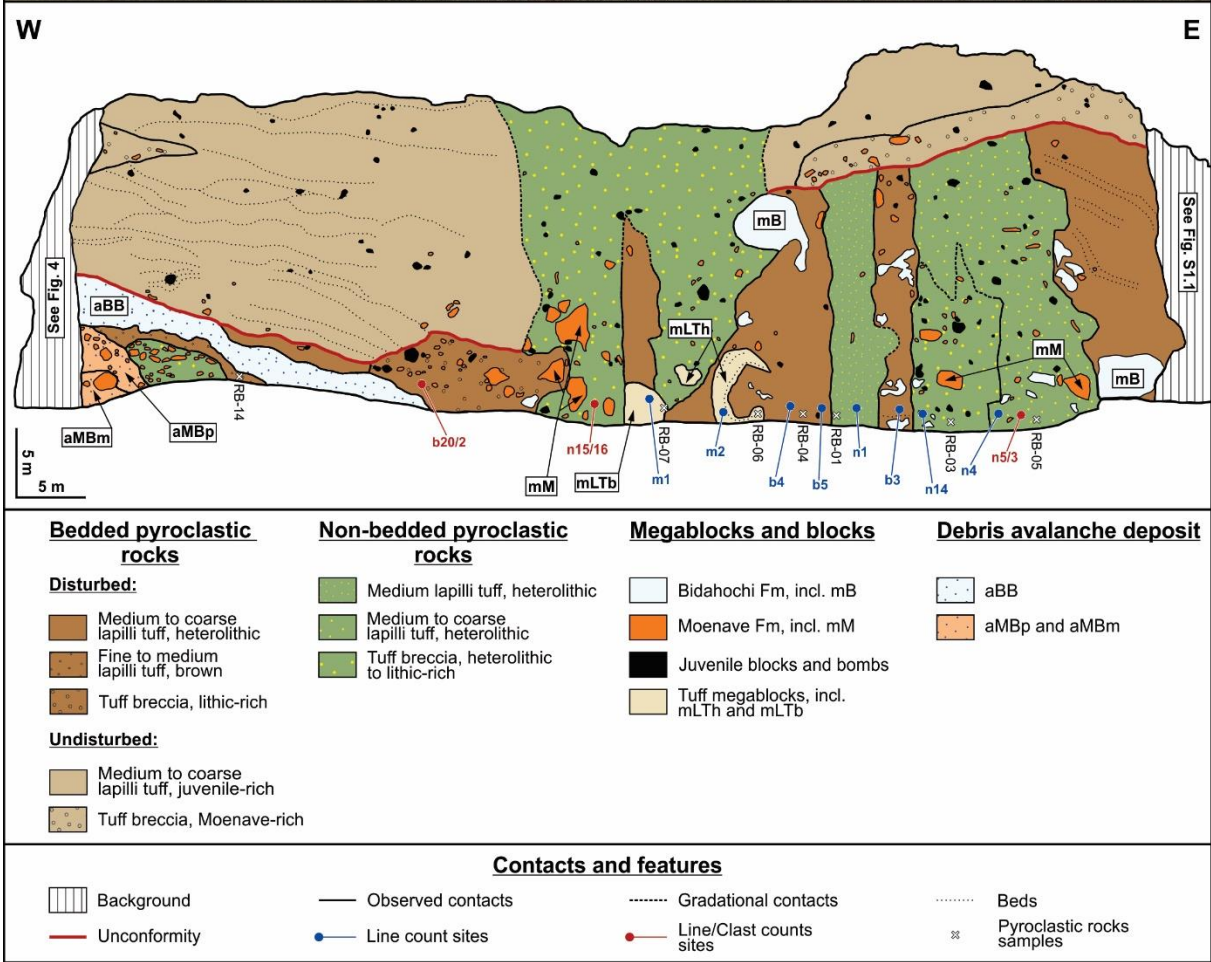
Figure 3 Geological map of the cliffs in the southern part of Round Butte (location in Fig. 1c) displaying three main groups of pyroclastic facies detailed in Latutrie and Ross (2019), the megablocks, and the debris avalanche deposits (DADs). For facies codes, see Table 1.
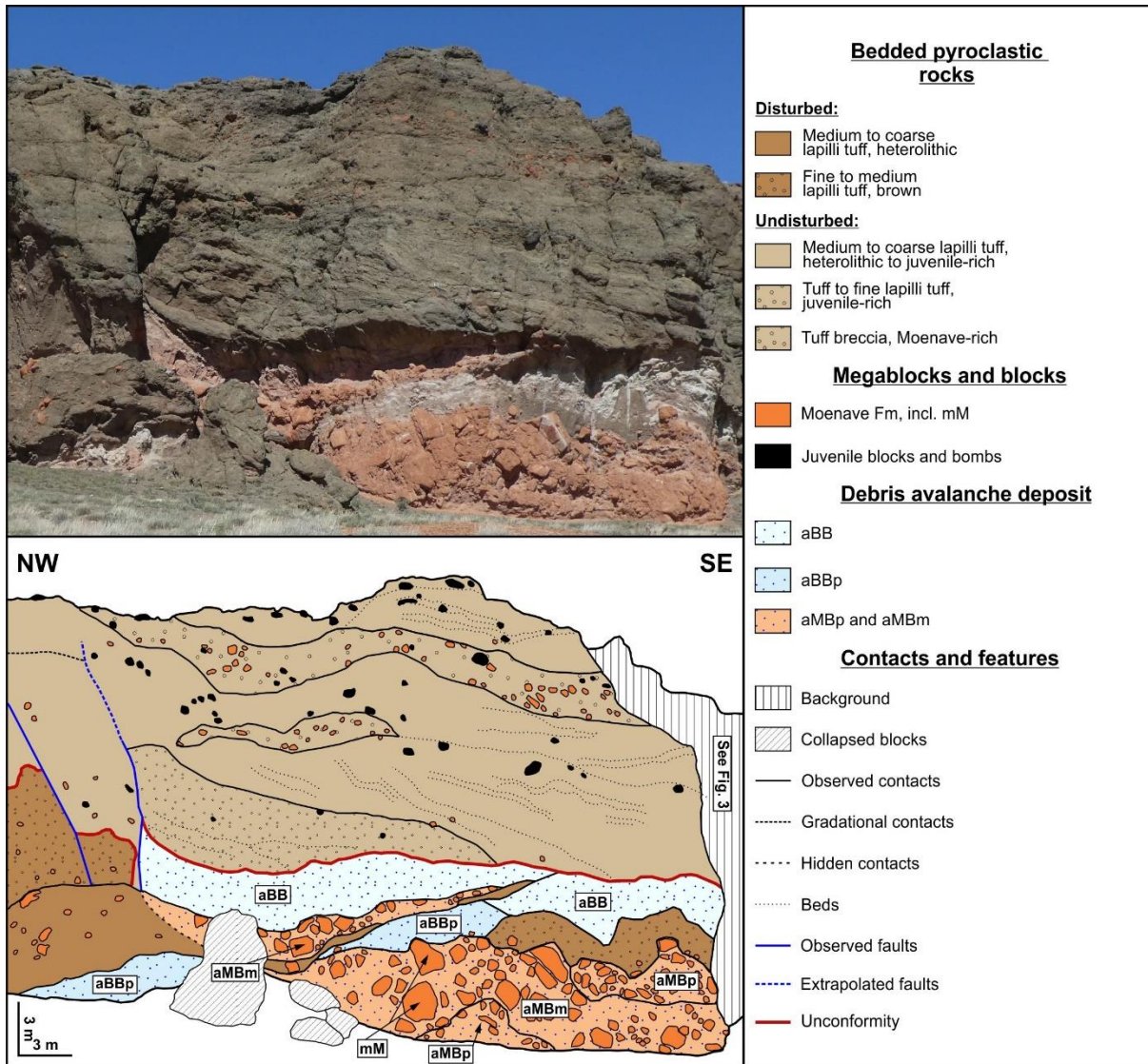
Figure 4 Geological map of the cliffs in the southwest part of Round Butte (location in Fig. 1c) displaying two main groups of facies detailed in Latutrie and Ross (2019), the megablocks, and the debris avalanche deposits (DADs). For facies codes, see and Table 1.
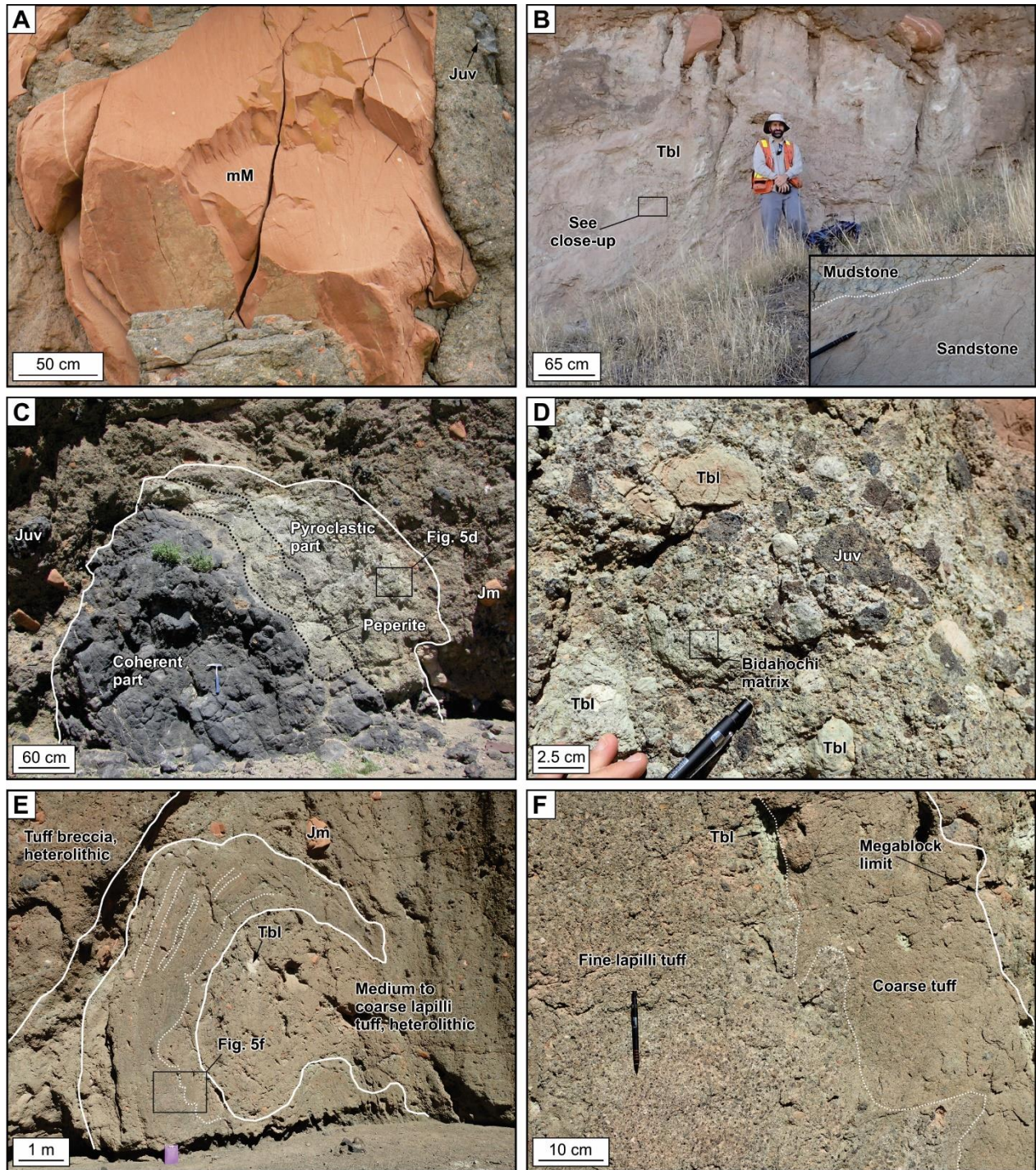
Figure 5 Photo plate of the megablocks. A) Red sandstone to siltstone from Moenave Formation (mM). B) Whitish sandstone to greenish mudstone from Bidahochi Formation (mB, Fig. S1.4). C) Composite mLTb megablock displaying a coherent lava part and a pyroclastic part separated by a peperitic zone. D) Close-up of the pyroclastic rock in the mLTb megablock, displaying a high content of Bidahochi clasts and brown to grey juvenile clasts, within a whitish matrix rich in disaggregated Bidahochi sediment. E) C-shape mLTh megablock composed of thin beds of coarse tuff to fine lapilli tuff. F) Close-up on the irregular contact of two beds in a mLTh megablock. For facies codes, see Table 1. Abbreviations: Tbl=Bidahochi clasts, Jm=Moenave clasts and Juv=Juvenile clasts.
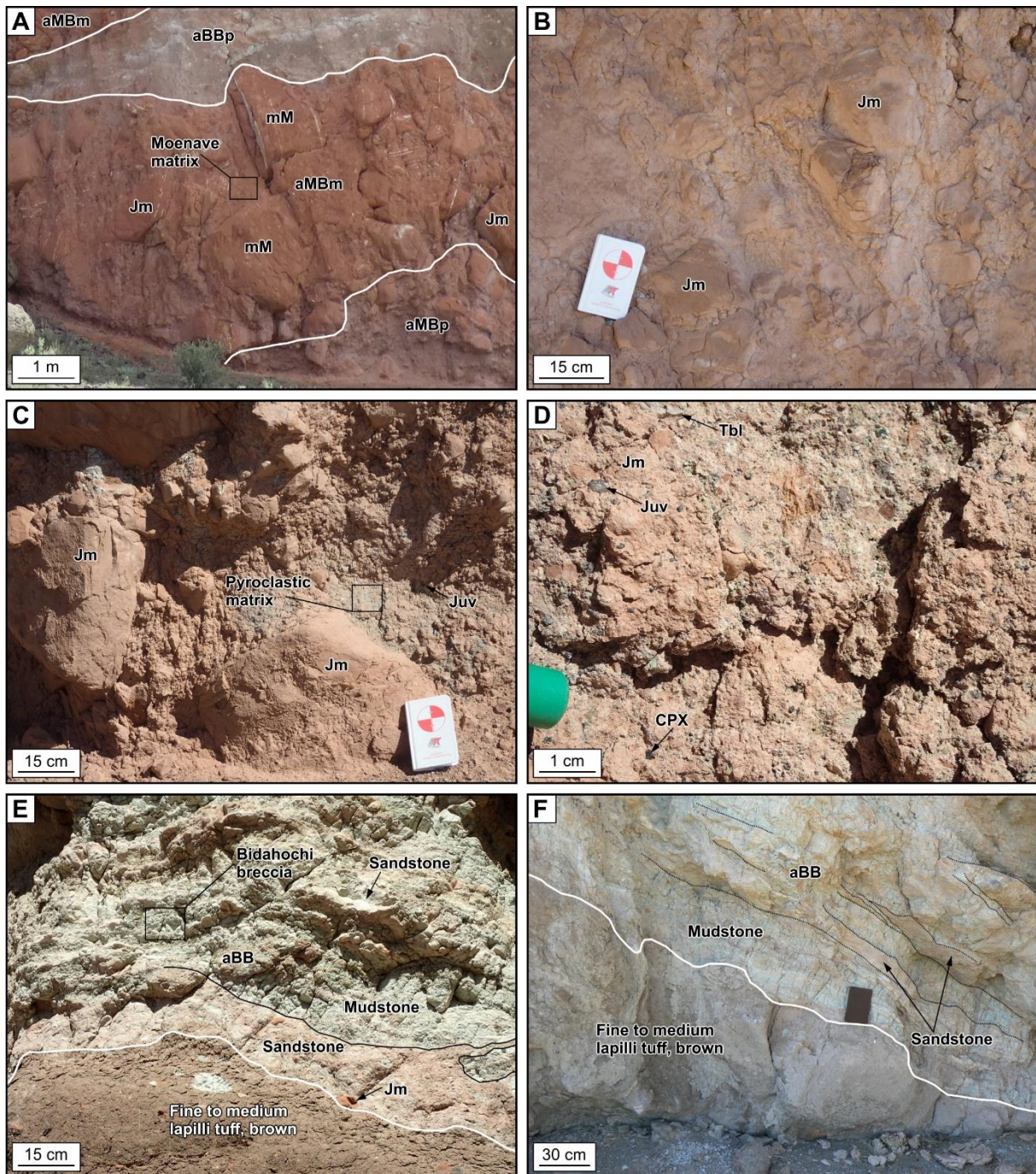
Figure 6 Photo plate of the facies in the main DAD. A) aMBm facies composed of Moenave megablocks and blocks, located between aMBp and aBBp facies. B) Close-up on the Moenave matrix of the aMBm facies. C) aMBp facies displaying a pyroclastic matrix between big blocks of Moenave Formation. D) Close-up on the pyroclastic matrix of the aMBp facies. E) More brecciated aBB facies just above a fine to medium lapilli tuff bed. F) Bedding in the aBB facies with remnants of beds of sandstone surrounded by mudstone. For facies codes, see Table 1. Abbreviations: Tbl=Bidahochi clasts, Jm=Moenave clasts, Juv=Juvenile clasts, CPX=free clinopyroxene.
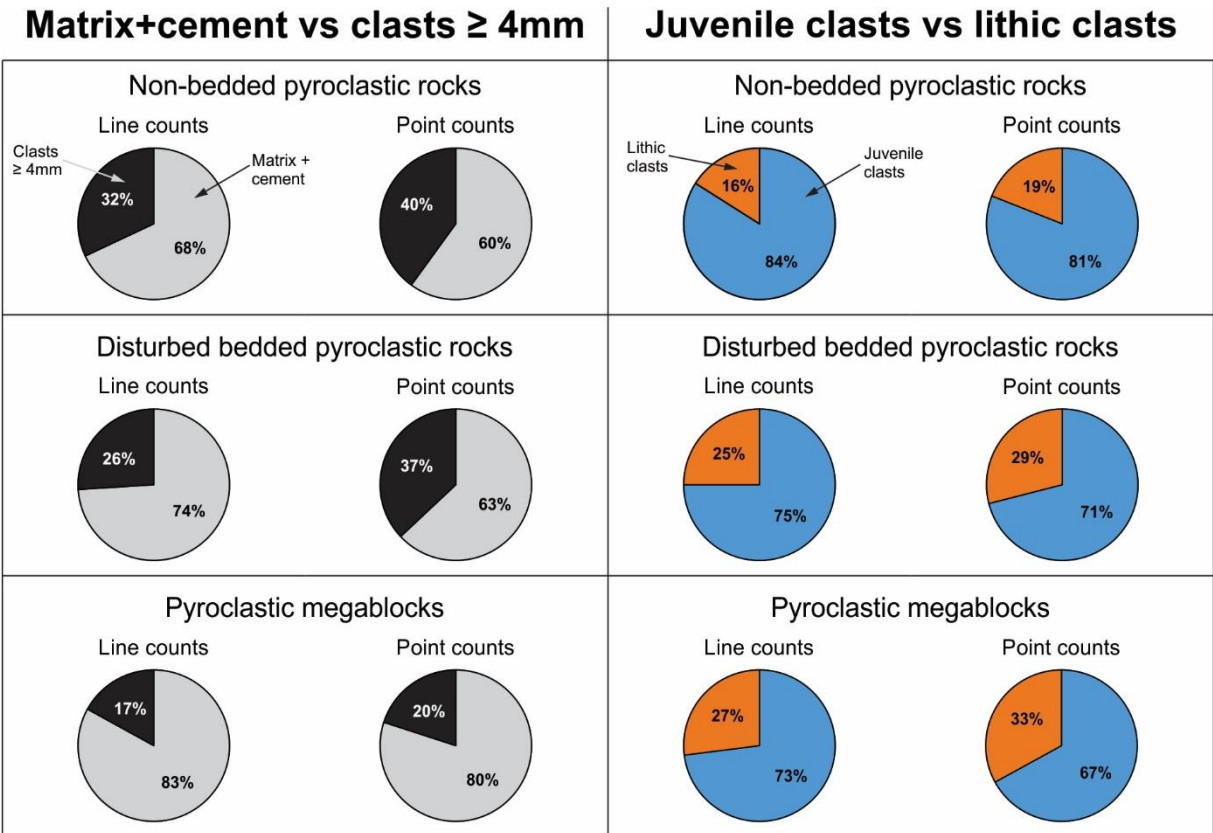
Figure 7 Field componentry data (line counts and point counts) plotted as average compositions on pie charts. The left column shows the proportions of matrix+cement (everything smaller than 4 mm) *vs* fragments 4 mm or larger. The right column shows the proportions of juvenile clasts *vs* country rock lithic clasts, among fragments 4 mm or larger. Note that the data presented here is detailed in Table 2 and Table 4. Online Resource 2 compares line counts and point counts at the same 15 sites only (Tables S2.1 and S2.2).
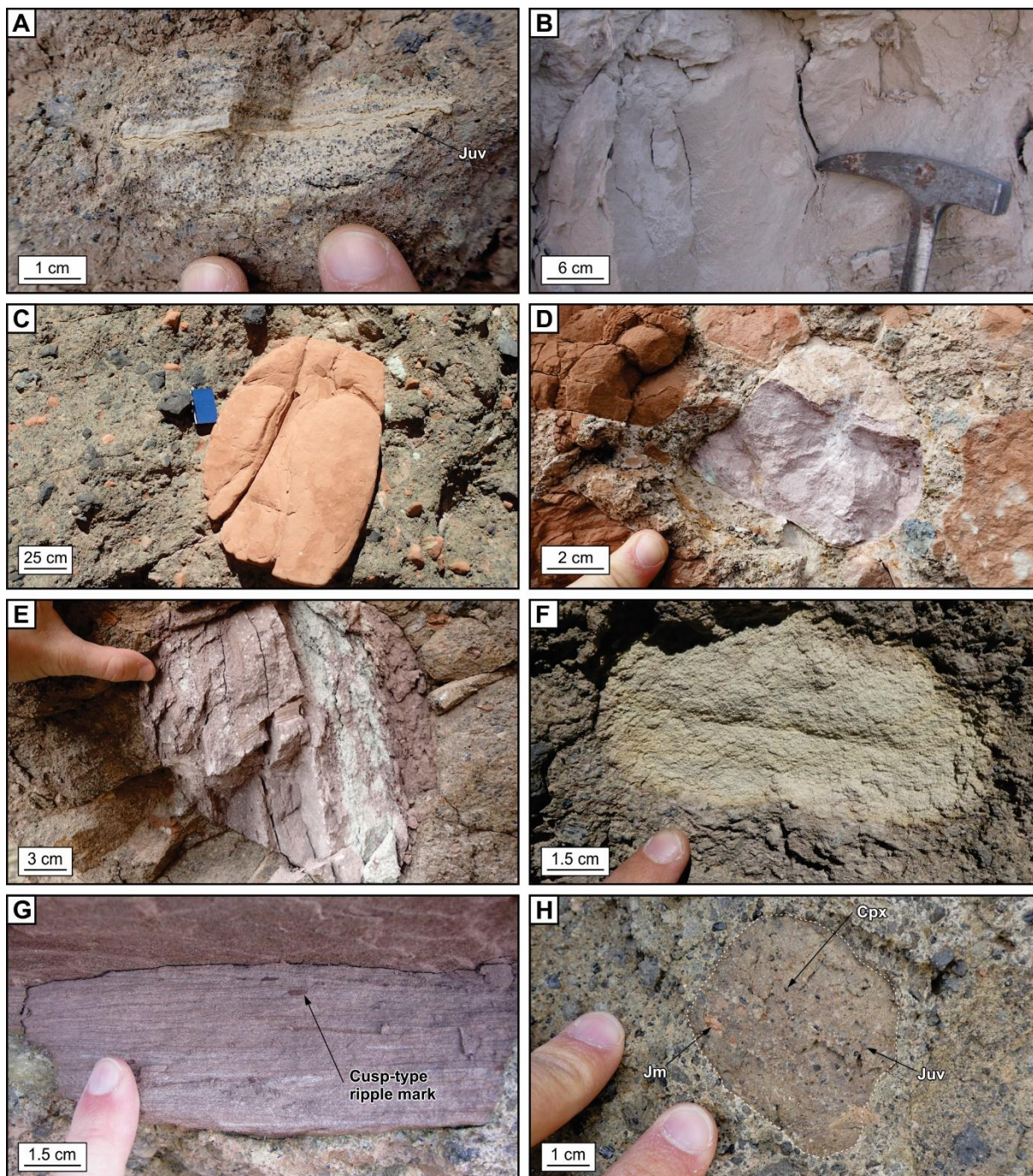
Figure 8 Photo plate showing the diversity of country rock lithic clasts, and a tuff clast, in the pyroclastic rocks of Round Butte. A) Finely bedded, juvenile-bearing clast from the Bidahochi Formation, B) whitish fine argillaceous sandstone of the Bidahochi Formation, C) reddish fine sandstone to siltstone of the Moenave Formation, D) purplish limestone of the Owl Rock Member of the Chinle Formation, E) purplish to whitish bedded siltstones of the Petrified Forest Member of the Chinle Formation, F) yellowish coarse sandstone of the Shinarump Member of the Chinle Formation, G) purplish-brown siltstone to sandstone of the Holbrook/Moqui Member of the Moenkopi Formation and H) sub-rounded tuff clast rich in juvenile and lithic (Moenave Formation) fragments. Abbreviations: Jm=Moenave clasts, Juv=Juvenile clasts, CPX=free clinopyroxene.
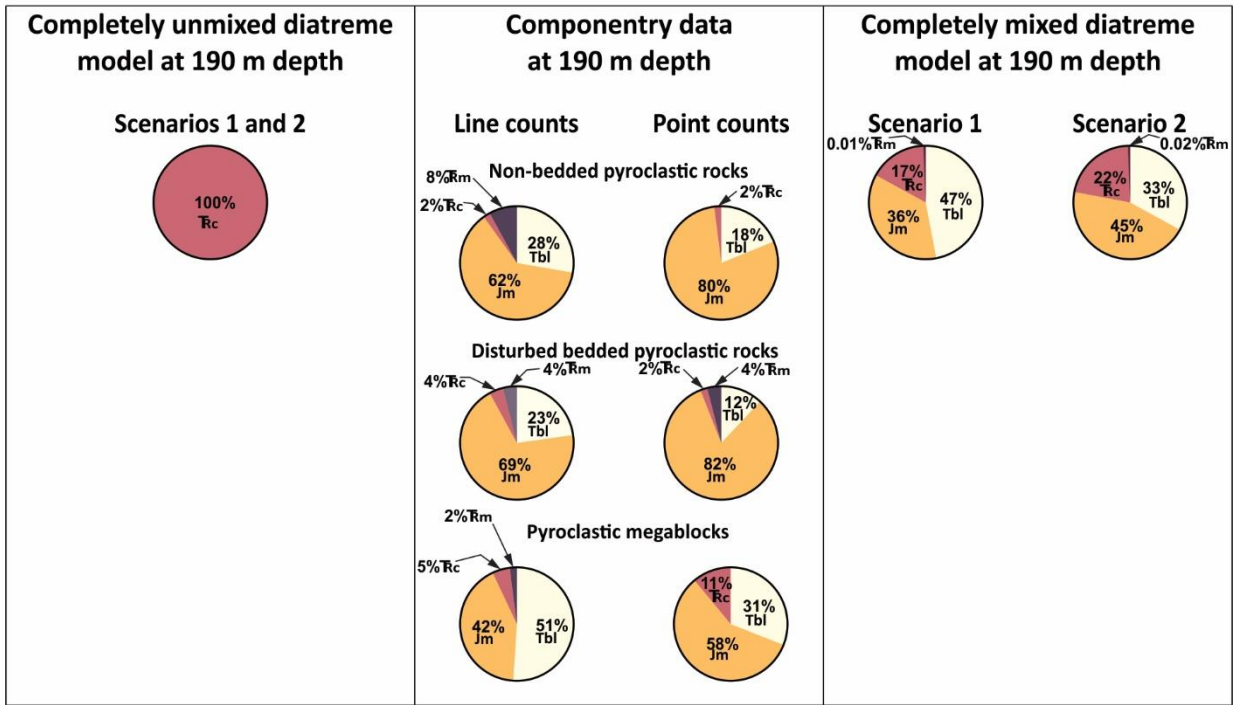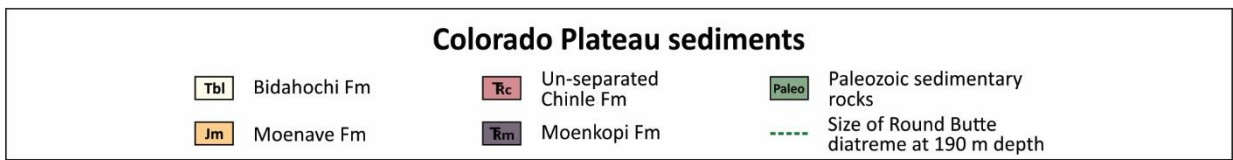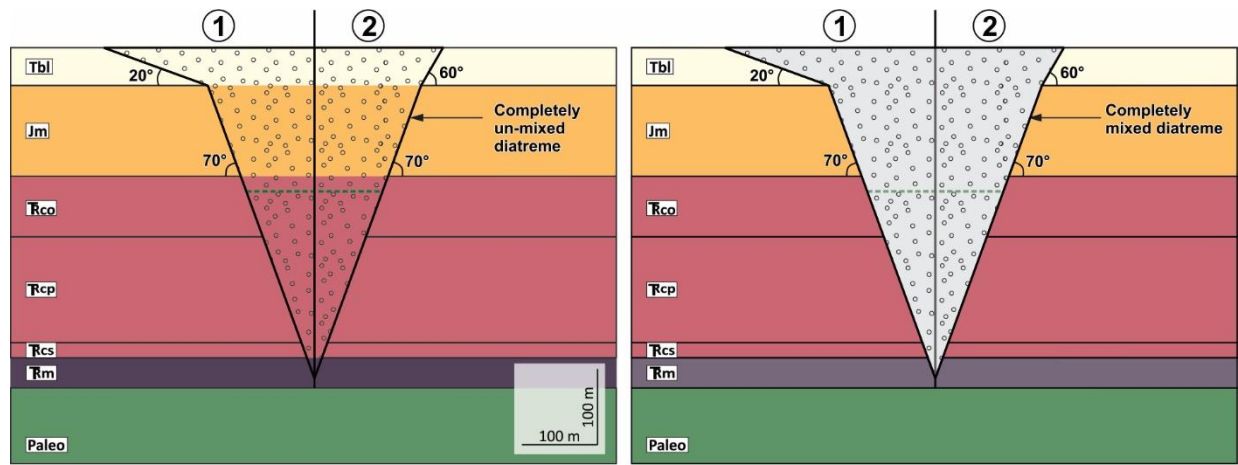
Figure 9 Scenarios of country rock fragmentation at Round Butte. Numbers 1 and 2 refer to the best scenarios tested (Table 6). The diatreme and the crater are drawn as filled by sedimentary rock formations (with dots) for the completely unmixed model (left) and by undifferentiated fill (grey with dot pattern) for the completely mixed model (right). These are extreme end-members which cannot explain the complex eruptive history of Round Butte (Latutrie and Ross, 2019), but are presented for illustrative purposes. This activity is characterized by two cycles of excavation and infilling of the crater, implying vertical movements of the crater floor during the eruption, unlike what is shown here. The line count data on this figure is not directly comparable with the point count data because they do not cover the same numbers of sites.

Table 1 Characteristics of megablocks and the debris avalanche deposits (DADs)

Facies code	Name	Description	Panoramas (Fig. nb)
Megablocks			
mM	Megablocks of Moenave Formation	Sub-rounded to angular, 5 m maximum size, homogeneous megablocks composed of orange fine sandstone to siltstone (Fig. 5a) sometimes with white spots or white lines.	3, 4, S1.1, S1.2, S1.4, S1.6, S1.7
mB	Megablocks of Bidahochi Formation (Lower and Middle)	Sub-rounded to irregular (liquefied) megablocks up to 7 m across. Mainly heterogeneous, composed of whitish to purplish fine sandstone to whitish to greenish mudstone (Fig. 5b). External parts are sometimes intruded by small tuff dikes (~cm- to dm- thick). Some megablocks display thin bands (cm-thick) rich in free pyroxenes and juvenile clasts.	3, S1.1 to S1.4, S1.6, S1.7
mC	Megablocks of Chinle Formation	Two megablocks (tens of meters) are preserved in pyroclastic rocks cropping out on floor around the Round Butte cliffs (Fig. 1c). They are not well exposed, are purplish in color and probably composed of sediments from the Owl Rock Member.	-
mJ	Juvenile megablocks	Sub-round to irregular very large juvenile bombs, vesicles are often filled by calcite or zeolites.	S1.1
mLTb	Composite megablock composed of two parts, lapilli tuff (Bidahochi-rich) and coherent lava part	Sub-rounded composite megablock ~3 m in diameter Coherent lava part (Fig. 5c): 10-15% serpentinized olivine, ~20% clinopyroxene, traces of phlogopite, 20-60% vesicles. At the contact with the pyroclastic part, diffuse jointing occurs. Pyroclastic part (Fig. 5d): 5% b&b (Juv ≈ Tbl), 50% lapilli (50-80% Juv and 20-50% Tbl), 43% ash (rich in Bidahochi mud and brown juvenile ash), 2% scattered cement. 50% of juvenile clasts are brown.	3
mLTh	Megablocks of lapilli tuff, heterolithic, bedded to non-bedded	Megablocks of 10 m maximum size, overall shape is elongated, sub-round, irregular or in 'c' (Figs. 5e, 5f). Within megablocks: 0-3% b&b (Tbl ≥ Jm > Juv), 15-60% lapilli (Juv ≥ Tbl, Jm, TRc, TRm), 54-80% ash (Juv and Lith), 0-15% cement. Traces of brown juvenile clasts. Local beds of coarse tuff, bed thickness from cm to m.	3, S1.2, S1.3, S1.6, S1.7
Debris avalanche deposits (DADs)			
Main DAD (Figs. 3, 4, 6)			
aMBm	Moenave breccia with a Moenave matrix	Moenave Formation brecciated into clasts mm to several meters across (Figs. 6a, 6b).	3, 4
aMBp	Moenave breccia with a pyroclastic matrix	Moenave Formation fragments (block- to lapilli-sized) with a pyroclastic matrix composed of grey juvenile clasts, free clinopyroxenes and Bidahochi clasts (Figs. 6c, 6d).	3, 4
aBB	Bidahochi breccia (bedded to remobilized)	Facies only composed of Bidahochi Formation clasts (block- to ash-sized) with brecciated to bedded parts (Figs. 6e, 6f). Beds are few cm- to m- thick, comprising greenish-white mudstone and purplish fine sandstone.	3, 4
aBBp	Bidahochi breccia with a pyroclastic matrix	Facies mainly composed of Bidahochi Formation clasts (block- to ash-sized) with an ash-rich pyroclastic matrix composed of Moenave and juvenile clasts.	3, S1.7
Minor DADs (Fig. 1.6)			
aTBh	Tuff breccia, heterolithic, with blocks of Moenave Fm and Bidahochi Fm	Facies that fills channels above the unconformity, composed of a mixture of Moenave, Bidahochi and juvenile clasts in a pyroclastic matrix.	S1.6

Juv = Juvenile clasts, Lith = Lithic clasts, Jm = Moenave Fm clasts, Tbl = Bidahochi Fm clasts, TRc = Chinle Fm clasts, TRm = Moenkopi Fm clasts, b&b = blocks and bombs

Table 2 Results of field line counts, expressed as percentages of clasts larger than, or equal to, 4 mm

Facies code[1]	Site umber	Panorama (Fig. nb)	Juvenile clasts								Country rock lithic clasts						Tuff clasts	Matrix (< 4 mm) + cement	L/(L+J)[2]
			Brown	Light grey	Medium grey	Dark grey	Black	Undiff.	CPX and phlogopite	Total	Bidahochi Fm	Moenave Fm	Chinle Fm	Moenkopi Fm	Undiff.	Total			
Disturbed bedded pyroclastic rocks																			
LTb	b1	S1.7	1.5	0.0	1.7	0.2	0.0	0.0	0.2	3.6	0.8	3.2	0.1	0.0	0.1	4.3	1.4	90.7	0.54
LTb	b2	S1.7	0.0	0.9	0.0	0.6	1.1	1.0	0.3	3.9	2.6	7.7	0.0	0.0	0.0	10.3	0.0	85.8	0.73
LTh	b3	3	0.7	1.9	3.4	6.1	2.0	0.5	0.3	14.9	6.3	9.1	0.0	1.3	0.2	16.9	0.0	68.2	0.53
LTh	b4	3	0.2	4.2	5.7	11.8	2.1	0.0	0.2	24.2	1.1	2.3	0.0	0.8	1.9	6.1	0.8	68.9	0.20
LTh	b5	3	0.2	1.4	3.7	6.7	0.9	0.0	0.1	13.0	0.8	2.5	0.0	0.9	1.1	5.3	3.9	77.8	0.29
LTh	b6	S1.4	0.5	8.1	4.5	10.3	0.6	0.0	0.3	24.3	7.2	3.6	0.5	0.0	0.5	11.8	0.0	63.9	0.33
LTh	b7	S1.7	2.5	2.8	1.9	17.6	3.0	0.4	0.3	28.5	0.0	3.8	0.0	0.1	2.5	6.4	0.0	65.1	0.18
LTh	b8	S1.7	0.6	0.5	1.1	11.2	7.1	0.5	0.0	21.0	0.0	7.5	1.0	0.1	0.3	8.9	0.0	70.1	0.30
LTh	b9	S1.6	0.3	1.3	7.1	5.5	0.0	0.0	0.0	14.2	0.4	1.3	0.0	0.0	0.2	1.9	0.0	83.9	0.12
LTh	b10	S1.6	0.0	2.8	4.2	5.8	0.0	0.8	0.1	13.7	0.3	0.7	0.0	0.0	0.9	1.9	0.0	84.4	0.12
LTh	b11	S1.1	0.3	1.3	4.6	11.2	2.1	0.0	0.7	20.2	0.0	4.8	0.0	0.0	0.0	4.8	0.0	75.0	0.19
LTh	b12	S1.1	0.0	1.7	5.9	14.6	1.6	0.0	0.0	23.8	3.8	1.2	0.4	0.0	0.2	5.6	0.0	70.6	0.19
LTh	b13	S1.2	0.2	1.2	3.1	16.2	3.5	0.0	0.1	24.3	0.2	6.2	0.0	0.0	0.3	6.7	0.0	69.0	0.22
LTh	b14	S1.2	0.0	2.1	6.7	8.5	2.6	0.0	0.3	20.2	0.4	3.0	0.0	1.0	0.0	4.4	0.0	75.4	0.18
LTh	b15	S1.2	1.0	8.5	5.0	4.2	0.3	3.6	0.5	23.1	0.0	7.5	0.0	0.0	0.2	7.7	0.0	69.2	0.25
LTh	b16	S1.3	1.6	1.7	4.2	13.8	0.4	1.4	1.3	24.4	0.6	1.8	0.0	0.0	0.4	2.8	0.0	72.8	0.10
LTh	b17	S1.3	0.1	2.8	8.3	16.5	1.4	0.0	0.0	29.1	0.7	3.8	0.0	0.0	0.1	4.6	0.0	66.3	0.14
LTh	b18	S1.3	0.0	0.5	1.8	12.9	8.4	0.6	0.3	24.5	0.0	1.4	0.0	0.3	0.8	2.5	0.0	73.0	0.09
LTh	b19	S1.3	0.4	3.5	10.8	12.5	1.3	0.2	0.8	29.5	0.1	2.1	0.2	0.0	0.0	2.4	0.0	68.1	0.08
TBl	b20	3	0.0	1.6	6.9	10.5	2.2	0.0	0.0	21.2	0.0	3.9	0.8	0.0	0.0	4.7	0.0	74.1	0.18
Mean	-	-	0.5	2.4	4.5	9.8	2.0	0.5	0.3	**20.1**	1.3	3.9	0.2	0.2	0.5	**6.0**	0.3	**73.6**	**0.25**
Non-bedded pyroclastic rocks																			
(m)LTh	n1	3	0.2	1.2	1.5	3.4	1.3	0.0	0.0	7.6	3.7	2.2	0.0	1.5	0.0	7.4	0.0	85.0	0.49
(m)LTh	n2	S1.4	0.3	1.6	3.5	5.7	0.9	0.1	1.1	13.2	1.6	0.5	0.0	0.0	0.3	2.4	0.0	84.4	0.15
(m)LTh	n3	S1.6	0.0	2.7	1.6	6.2	0.0	0.3	0.0	10.8	0.0	0.3	0.0	0.0	0.0	0.3	0.0	88.9	0.03
(mc)LTh	n4	3	0.0	1.2	10.4	10.7	5.9	0.0	0.4	28.6	2.0	2.8	0.0	0.2	0.0	5.0	1.3	65.1	0.15
(mc)LTh	n5	3	0.9	1.3	4.8	15.5	1.2	0.0	0.1	23.8	11.7	9.5	0.0	0.0	0.0	21.2	1.3	53.7	0.47

Facies	Sample	Code																	L/(L+J)
(mc)LTh	n6	S1.4	1.2	5.1	3.7	13.6	0.5	0.0	0.3	24.4	0.1	4.5	0.0	0.0	0.3	4.9	0.0	70.7	0.17
(mc)LTh	n7	S1.6	0.0	3.5	8.9	9.2	0.2	0.0	0.0	21.8	0.0	6.6	0.4	0.0	0.3	7.3	0.8	70.1	0.25
(mc)LTh	n8	S1.3	1.2	5.7	6.5	17.0	2.9	0.2	0.8	34.3	0.6	0.4	0.0	0.0	0.2	1.2	0.0	64.5	0.03
(mc)LTh	n9	S1.3	0.7	5.9	6.3	11.3	0.6	0.1	0.3	25.2	1.1	0.0	0.0	0.8	0.0	1.9	0.0	72.9	0.07
(mc)LTh	n10	S1.5	1.2	1.4	4.4	30.3	2.1	0.0	0.5	39.9	0.2	1.0	0.0	0.0	0.5	1.7	0.0	58.4	0.04
(c)LTj	n11	S1.4	1.7	2.5	5.8	22.1	4.4	0.0	0.7	37.2	0.7	1.4	0.0	0.0	0.2	2.3	0.0	60.5	0.06
(c)LTj	n12	S1.4	0.3	4.2	4.7	18.2	0.7	0.0	0.2	28.3	0.0	0.4	0.0	0.0	0.1	0.5	0.5	70.7	0.02
(c)LTj	n13	S1.4	0.4	3.9	4.6	22.9	0.7	0.3	1.1	33.9	0.7	0.3	0.2	0.0	0.0	1.2	0.0	64.9	0.03
TBh	n14	3	0.4	1.6	8.1	6.2	8.0	0.7	0.1	25.1	0.6	13.5	0.0	4.6	0.3	19.0	0.0	55.9	0.43
TBh	n15	3	0.9	8.0	11.5	11.3	0.0	0.0	0.0	31.7	0.6	6.3	0.6	0.0	0.3	7.8	0.7	59.8	0.20
TBh	n16	S1.4	0.6	2.8	6.8	31.6	1.2	0.2	0.6	43.8	0.5	2.0	0.0	0.0	0.0	2.5	0.0	53.7	0.05
TBh	n17	S1.1	0.3	1.8	4.3	13.7	4.0	0.6	0.5	25.2	0.0	2.6	0.0	0.2	0.5	3.3	0.0	71.5	0.12
Mean	-	-	0.6	3.2	5.7	14.6	2.0	0.1	0.4	**26.8**	1.4	3.2	0.1	0.4	0.2	**5.3**	0.3	**67.7**	**0.16**
Pyroclastic megablocks																			
mLTb	m1	3	3.3	1.2	2.2	8.2	0.6	5.0	0.6	21.1	2.5	0.0	0.0	0.0	0.0	2.5	0.0	76.4	0.11
mLTh	m2	3	2.2	0.7	2.0	4.4	2.4	0.0	0.3	12.0	2.8	0.4	0.7	0.2	0.1	4.2	0.0	83.8	0.26
mLTh	m3	S1.6	0.0	0.6	1.4	8.3	1.8	0.2	0.6	12.9	0.2	0.8	0.6	0.0	0.2	1.8	0.0	85.3	0.12
mLTh	m4	S1.2	0.1	0.1	0.6	4.2	4.7	0.5	0.3	10.5	0.0	2.2	0.0	0.2	0.9	3.3	0.0	86.2	0.24
mLTh	m5	S1.3	0.0	4.3	5.4	1.2	0.0	0.0	0.2	11.1	4.4	2.7	0.0	0.0	0.0	7.1	0.0	81.8	0.39
mLTh	m6	S1.3	0.0	3.7	3.4	0.8	0.1	0.1	0.2	8.3	2.9	4.2	0.0	0.0	0.7	7.8	1.2	82.7	0.48
Mean	-	-	0.9	1.8	2.5	4.5	1.6	1.0	0.4	**12.7**	2.1	1.7	0.2	0.1	0.3	**4.5**	0.2	**82.7**	**0.27**

[1] Facies codes for disturbed bedded pyroclastic rocks and the non-bedded pyroclastic rocks are decomposed into parts as follows: (m) = medium, (mc) = medium to coarse, (c) = coarse; LT = Lapilli tuff, TB = Tuff Breccia; b = brown, h = heterolithic, l = lithic-rich and j = juvenile-rich. See Table 1 for pyroclastic megablocks facies codes.

[2] L/(L+J) is the relative proportion of country rock lithic (L) fragments, relative to the sum of country rock lithic clasts and juvenile (J) fragments.

Table 3 Mann-Witney U Test[1] on componentry data for different facies groups

	Matrix + cement[2]			L/(L+J)[3]		
	Disturbed bedded rocks	Non-bedded rocks	Pyroclastic megablocks	Disturbed bedded rocks	Non-bedded rocks	Pyroclastic megablocks
Line counts						
Disturbed bedded rocks	-	-	-	-	-	-
Non-bedded rocks	N[4]	-	-	**Y[4]**	-	-
Pyroclastic megablocks	**Y**	**Y**	-	N	N	-
Field point counts						
Disturbed bedded rocks	-	-	-	-	-	-
Non-bedded rocks	N	-	-	N	-	-
Pyroclastic megablocks	N	N	-	N	N	-
Petrographic point counts						
Disturbed bedded rocks	-	-	-	-	-	-
Non-bedded rocks	-	-	-	N	-	-
Pyroclastic megablocks	-	-	-	N	N	-

[1] Null hypothesis for the statistical test: the two "groups" (here componentry datasets for different facies groups) come from populations with equal distributions (i.e., the difference in group distributions could be due to random sampling variability alone). Alternative hypothesis: the populations have different distributions. Significance level: 0.05.

[2] Matrix + cement is the proportion of material not consisting of clasts 4 mm or larger in the field componentry. Not applicable to petrographic point counts.

[3] L/(L+J) is the relative proportion of country rock lithic (L) fragments, relative to the sum of country rock lithic clasts and juvenile (J) fragments.

[4] **Y** = Yes, there is a significant difference in distributions (we reject the null hypothesis and accept the alternative, i.e., the populations are different); N = there is not a significant difference in distributions (we fail to reject the null hypothesis). Note that 'N' does not mean that the populations are *proven* to be the same. They could still be different, but there is not enough data to show it, given the small sample sizes and large standard deviations.

Table 4 Results of field point counts, expressed as percentages of clasts larger than, or equal to, 4 mm

Facies code [1]	Line count sites	Panorama (Fig. nb)	Point count sites	Juvenile clasts								Country rock lithic clasts						Tuff clasts	Cement	Matrix (<4 mm)	L/(L+J) [2]	Stdev (1σ) [3]
				Brown	Light grey	Medium grey	Dark grey	Black	Undiff.	CPX and phlogopite	Total	Bidahochi Fm	Moenave Fm	Chinle Fm	Moenkopi Fm	Undiff.	Total					
Disturbed bedded pyroclastic rocks																						
LTh	b7	S1.7	14	3.3	1.1	12.1	5.5	5.5	0.0	0.0	27.5	0.0	2.2	0.0	1.1	0.0	3.3	0.0	3.3	65.9	0.11	0.06
LTh	b8	S1.7	15	0.0	0.0	8.9	6.9	0.0	0.0	0.0	15.8	0.0	17.8	1.0	1.0	1.0	20.8	0.0	6.9	56.4	0.57	0.08
LTh	b17	S1.3	8	3.5	2.4	20.0	5.9	2.4	0.0	2.4	36.5	4.7	3.5	0.0	0.0	0.0	8.2	0.0	2.4	52.9	0.18	0.06
LTh	b19	S1.3	5	1.2	4.7	12.8	10.5	0.0	0.0	1.2	30.2	1.2	8.1	0.0	0.0	1.2	10.5	0.0	12.8	46.5	0.26	0.07
TBl	b20	3	2	1.0	7.1	7.1	7.1	0.0	0.0	0.0	22.4	0.0	10.2	0.0	0.0	0.0	10.2	1.0	0.0	66.3	0.31	0.08
Mean	-	-	-	1.8	3.0	12.2	7.2	1.6	0.0	0.7	**26.5**	1.2	8.4	0.2	0.4	0.4	**10.6**	0.2	5.1	57.6	**0.29**	**0.07**
Non-bedded pyroclastic rocks																						
(mc)LTh	n5	3	3	0.0	8.0	3.0	2.0	16.0	0.0	0.0	29.0	3.0	9.0	1.0	0.0	0.0	13.0	0.0	0.0	58.0	0.31	0.07
(mc)LTh	n7	S1.6	12	7.4	1.1	12.8	12.8	8.5	0.0	0.0	42.6	1.1	5.3	0.0	0.0	1.1	7.4	0.0	2.1	47.9	0.15	0.05
(mc)LTh	n8	S1.3	9	2.0	11.2	9.2	12.2	3.1	0.0	0.0	37.8	0.0	7.1	0.0	0.0	0.0	7.1	0.0	17.3	37.8	0.16	0.05
(c)LTj	n11	S1.4	11	0.0	5.0	6.0	5.0	1.0	0.0	0.0	17.0	0.0	2.0	0.0	0.0	1.0	3.0	0.0	4.0	76.0	0.15	0.08
(c)LTj	n12	S1.4	10	5.7	11.4	2.3	10.2	17.0	0.0	0.0	46.6	1.1	3.4	0.0	0.0	0.0	4.5	0.0	8.0	40.9	0.09	0.04
TBh	n15	3	16	0.0	8.9	11.1	16.7	3.3	0.0	0.0	40.0	1.1	6.7	0.0	0.0	1.1	8.9	2.2	2.2	46.7	0.18	0.06
TBh	n17	S1.1	4	0.0	1.0	4.0	5.1	3.0	0.0	0.0	13.1	2.0	3.0	0.0	0.0	0.0	5.1	0.0	0.0	81.8	0.28	0.11
Mean	-	-	-	2.2	6.7	6.9	9.1	7.4	0.0	0.0	**32.3**	1.2	5.2	0.1	0.0	0.5	**7.0**	0.3	4.8	55.6	**0.19**	**0.07**
Pyroclastic megablocks																						
mLTh	m3	S1.6	13	0.0	4.0	4.0	2.0	3.0	0.0	0.0	13.1	0.0	2.0	0.0	0.0	0.0	2.0	0.0	0.0	84.8	0.13	0.09
mLTh	m5	S1.3	6	0.0	5.9	8.9	1.0	0.0	0.0	1.0	16.8	0.0	4.0	1.0	0.0	1.0	5.9	0.0	0.0	77.2	0.26	0.09
mLTh	m6	S1.3	7	0.0	3.0	1.0	3.0	0.0	0.0	1.0	8.0	6.0	5.0	1.0	0.0	0.0	12.0	2.0	0.0	78.0	0.60	0.11
Mean	-	-	-	0.0	4.3	4.7	2.0	1.0	0.0	0.7	**12.7**	2.0	3.7	0.7	0.0	0.3	**6.7**	0.7	0.0	80.0	**0.33**	**0.10**

[1] Facies codes for disturbed bedded pyroclastic rocks and the non-bedded pyroclastic rocks are decomposed into parts as follows: (m) = medium, (mc) = medium to coarse, (c) = coarse; LT = Lapilli tuff, TB = Tuff Breccia; b = brown, h = heterolithic, l = lithic-rich and j = juvenile-rich. See Table 1 for pyroclastic megablocks facies codes.

[2] L/(L+J) is the relative proportion of country rock lithic (L) fragments, relative to the sum of country rock lithic clasts and juvenile (J) fragments.

[3] Standard deviation representing a theoretical counting error on L/(L+J), calculated using the equation proposed by van der Plas and Tobi (1965), based on the measured proportion and the number of points falling on juvenile and country lithic clasts 4 mm or more across (n_{eff}), which ranges from 31 to 45 for the disturbed bedded rocks, from 18 to 52 for the non-bedded rocks, and from 15 to 23 for the pyroclastic megablocks.

Table 5 Results of petrographic point counts measurements, expressed as modal percentages

			Juvenile clasts							Country rock lithic clasts										
Facies code[1]	Sample	Panorama (Fig. nb)	Brown	Light grey[2]	Grey (medium to dark)	Black	Undiff.	CPX and phlogopite	Total	Sandstone	Siltstone	Mudstone	Quartz	Total	Tuff clasts	Calcite cement	Void[3]	Unresolved	L/(L+J)[4]	Stdev (1σ)[5]
Disturbed bedded pyroclastic rocks																				
T	RB-40	S1.4	9.3	25.3	6.4	0.4	7.3	5.3	54.2	0.0	4.7	3.8	2.0	10.5	0.0	1.1	0.7	33.6	0.16	0.02
LTb	RB-14	3	6.0	9.6	16.4	2.4	4.7	2.7	41.8	0.7	2.4	0.0	2.4	5.6	0.0	0.0	2.7	50.0	0.12	0.02
LTb	RB-18	S1.7	0.7	22.7	6.4	4.4	0.4	2.7	37.3	0.0	4.4	3.8	6.4	14.7	0.0	1.3	1.3	45.4	0.28	0.03
LTh	RB-04	3	1.3	15.8	37.6	4.7	2.7	2.7	64.7	0.0	1.3	2.0	1.1	4.4	0.0	11.8	0.4	18.7	0.06	0.01
LTh	RB-33	S1.3	5.3	14.2	23.3	8.0	1.6	7.6	60.0	0.0	0.4	0.2	0.4	1.1	0.0	14.0	2.4	22.5	0.02	0.01
LTh	RB-16	S1.7	4.9	14.9	22.9	8.0	3.8	1.8	56.2	0.9	5.8	1.6	1.3	9.6	0.0	8.7	0.0	25.6	0.15	0.02
Mean	-	-	3.6	17.1	18.9	4.7	3.4	3.8	**52.4**	0.3	3.2	1.9	2.3	**7.6**	0.0	6.1	1.3	**32.6**	**0.13**	**0.02**
Non-bedded pyroclastic rocks																				
(m)LTh	RB-01	3	9.3	27.8	17.1	0.4	8.7	3.1	66.4	0.0	2.4	1.1	0.7	4.2	0.0	23.3	0.4	5.6	0.06	0.01
(m)LTh	RB-38	S1.4	2.7	9.1	25.6	7.1	3.6	3.6	51.6	0.0	2.7	1.6	2.9	7.1	0.0	1.3	2.9	37.1	0.12	0.02
(mc)LTh	RB-05	3	5.1	14.7	22.2	1.1	5.3	5.6	54.0	0.0	8.9	0.7	0.9	10.5	0.0	4.7	0.7	30.2	0.16	0.02
(mc)LTh	RB-43	S1.4	13.6	16.2	11.3	0.2	3.6	7.6	52.5	0.0	3.6	1.1	2.0	6.7	0.0	0.2	0.4	40.2	0.11	0.02
(mc)LTh	RB-26	S1.5	5.1	16.9	26.9	6.4	2.0	3.1	60.4	0.0	2.7	1.3	2.4	6.4	0.0	20.7	0.2	12.2	0.10	0.02
(c)LTj	RB-37	S1.4	11.1	20.4	20.7	2.2	1.8	7.1	63.3	0.0	1.1	0.4	0.4	2.0	0.0	9.8	0.2	24.7	0.03	0.01
(c)LTj	RB-42	S1.4	7.1	5.6	23.8	16.0	2.9	4.7	60.0	0.0	0.9	1.3	0.4	2.7	0.0	15.1	0.4	21.8	0.04	0.01
TBh	RB-03	3	2.4	31.8	13.1	5.8	3.6	2.7	59.3	0.0	6.2	2.2	1.3	9.8	0.0	10.9	0.0	20.0	0.14	0.02
TBh	RB-39	S1.4	2.7	14.9	35.6	3.1	0.7	2.4	59.3	1.8	2.9	2.7	1.8	9.1	0.0	10.2	0.2	21.1	0.13	0.02
Mean	-	-	6.6	17.5	21.8	4.7	3.6	4.4	**58.5**	0.2	3.5	1.4	1.4	**6.5**	0.0	10.7	0.6	**23.7**	**0.10**	**0.02**
Pyroclastic megablocks																				
mLTb	RB-07	3	35.8	3.1	19.0	1.1	2.9	3.3	65.2	0.0	3.6	1.3	0.2	5.1	0.0	15.8	2.0	11.9	0.07	0.01
mLTh	RB-06	3	12.9	13.3	20.0	1.3	3.8	4.4	55.8	0.0	1.8	1.8	5.6	9.1	0.0	1.8	0.0	33.3	0.14	0.02
mLTh	RB-34	S1.3	4.4	8.9	6.9	1.6	3.8	3.6	29.1	1.1	7.3	6.7	5.3	20.4	1.8	0.9	1.8	46.0	0.41	0.03
Mean	-	-	17.7	8.4	15.3	1.3	3.5	3.8	**50.0**	0.4	4.2	3.3	3.7	**11.6**	0.6	6.2	1.3	**30.4**	**0.21**	**0.02**

[1] Facies codes for disturbed bedded pyroclastic rocks and the non-bedded pyroclastic rocks are decomposed into parts as follows: (m) = medium, (mc) = medium to coarse, (c) = coarse; T = Tuff, LT = Lapilli tuff, TB = Tuff Breccia; b = brown, h = heterolithic, l = lithic-rich and j = juvenile-rich. See Table 1 for pyroclastic megablocks facies codes.

[2] Clasts that are "light grey" in the field or in polished slabs are dark brown petrographically.

[3] The void category is composed the porosity of the rock, some of which might be related to the thin section-making process.

[4] L/(L+J) is the relative proportion of country rock lithic (L) fragments, relative to the sum of country rock lithic clasts and juvenile (J) fragments.

[5] Standard deviation, representing a theoretical counting error on L/(L+J), calculated using the equation proposed by van der Plas and Tobi (1965), based on the measured proportion and the number of points falling on identifiable juvenile and country lithic clasts and minerals (n_{eff}), which ranges from 213 to 311 for the disturbed bedded rocks, from 264 to 318 for the non-bedded rocks, and from 223 to 316 for the pyroclastic megablocks.

Table 6 Comparison of the country rock fragmentation model with country rock lithic proportions in line and field point counts[1]

	Bidahochi Fm	Moenave Fm	Chinle Fm	Moenkopi Fm	Paleozoic seds.[2]	Total
Volume fragmented unmixed and mixed diatreme models ($x10^6\,m^3$)						
Scenario 1	7.1	5.3	2.6	0.002	0.00	14.9
Scenario 2	3.8	5.3	2.6	0.002	0.00	11.7
'Theoretical' proportion of fragmented formations at 190 m depth (country rock lithic clast %)						
Unmixed diatreme models (Fig. 9)						
Scenario 1	0	0	100	0	0	100
Scenario 2	0	0	100	0	0	100
Mixed diatreme models (Fig. 9)						
Scenario 1	47	36	17	0.01	0.0	100
Scenario 2	33	45	22	0.02	0.0	100
Mean (1 & 2)	40	40	19	0.02	0.0	100
Field line counts at 43 sites at 190 m depth (Table 2; country rock lithic clast %)						
Facies groups[3]						
Disturbed bedded group	23	69	4	4	0	100
Non-bedded group	28	62	2	8	0	100
Pyroclastic megablocks	51	42	5	2	0	100
Field point counts at 15 sites at 190 m depth (Table 4; country rock lithic clast %)						
Facies groups[3]						
Disturbed bedded group	12	82	2	4	0	100
Non-bedded group	18	80	2	0	0	100
Pyroclastic megablocks	31	58	11	0	0	100

[1]All percentages are recalculated on a 100% country rock lithic clasts basis.

[2]Paleozoic sedimentary rocks (Billingsley et al., 2013).

[3]Facies groups are described in Latutrie and Ross (2019) and Table 1.